PERFORMANCE OF GO/ZnO/EPOXY NANO COMPOSITE COATING WITH CORROSION RESISTANCE FOR MAGNISUM ALLOY IN SALINE SOLUTION

2025
MASTER THESIS
MECHANICAL ENGINEERING

Khaled ALJILOU

Thesis Advisor
Assist. Prof. Dr. Khaled.M.N. CHAHROUR

PERFORMANCE OF GO/ZNO/EPOXY NANO COMPOSITE COATING WITH CORROSION RESISTANCE FOR MAGNISUM ALLOY IN SALINE SOLUTION

Khaled ALJILOU

Thesis Advisor
Assist. Prof. Dr. Khaled.M.N. CHAHROUR

T.C.
Karabuk University
Institute of Graduate Programs
Department of Mechanical Engineering
Prepared as
Master Thesis

KARABUK
Mayıs 2025

I certify that in my opinion, the thesis submitted by Khaled ALJILOU titled "PERFORMANCE OF GO/ZNO/EPOXY NANO COMPOSITE COATING WITH CORROSION RESISTANCE FOR MAGNISUM ALLOY IN SALINE SOLUTION" is fully adequate in scope and in quality as a thesis for the degree of Master of Science.

Assist. Prof. Dr. Khaled M.N CHAHROUR .....
Thesis Advisor, Department of Mechanical Engineering

This thesis is accepted by the examining committee with a unanimous vote in the Department of Mechanical Engineering as a Master of Science thesis. May 30, 2025

Examining Committee Members (Institutions)	Signature
Chairman : Assist. Prof. Dr. Ammar ALSHEMARY (WKU)	.....
Member : Assist. Prof. Dr. Sena KABAVE KILINÇARSLAN (KBU)	.....
Member : Assist. Prof. Dr. Khaled M.N CHAHROUR (KBU)	.....

The degree of Master of Science by the thesis submitted is approved by the Administrative Board of the Institute of Graduate Programs, Karabuk University.

Assoc. Prof. Dr. Zeynep ÖZCAN .....
Director of the Institute of Graduate Programs

"I declare that all the information within this thesis has been gathered and presented in accordance with academic regulations and ethical principles and I have according to the requirements of these regulations and principles cited all those which do not originate in this work as well."

Khaled ALJILOU

ABSTRACT

Master Thesis

PERFORMANCE OF GO/ZNO/EPOXY NANO COMPOSITE COATING WITH CORROSION RESISTANCE FOR MAGNISUM ALLOY IN SALINE SOLUTION

Khaled ALJILOU

Karabük University
Institute of Graduate Programs
Department of Mechanical Engineering

Thesis Advisor:
Assist. Prof. Dr. Khaled. M. N. CHAHROUR
Mayıs 2025, 75 pages

This study explores the enhancement of anti-corrosive performance in epoxy resin coatings by incorporating ZnO nanoparticles and their modification with graphene oxide (GO). Various ZnO and GO weight percentages were optimized to develop a ZnO/GO nanocomposite as an efficient barrier within the epoxy matrix. The most notable improvement was observed with 4.10 wt% ZnO and 0.05 wt% GO ($ZnO_{4.1}/GO_{0.05}$), achieving a significant corrosion current rate (CR) of 4.170 mmpy, and a remarkable transfer resistance (R_{ct}) of 499020 $\Omega.cm^{-2}$. These values are significantly higher than those of coatings modified with only ZnO nanoparticles (CR of 43.54 mmpy, R_{ct} of 129000 $\Omega.cm^{-2}$) and pure epoxy coatings (CR of 854.4 mmpy, R_{ct} of 54232 $\Omega.cm^{-2}$), respectively. The anti-corrosion performance of the $ZnO_{4.10}/GO_{0.05}$ coating was further validated after 72 hours of immersion in a 3.5% NaCl solution, demonstrating superior resistance to degradation compared to other

formulations. Morphological, structural, thermal, and surface properties of the prepared coatings were characterized using Field Emission Scanning Electron Microscopy (FESEM) coupled with energy-dispersive X-ray spectroscopy (EDX), Thermogravimetric Analysis (TGA), Fourier-transform infrared spectroscopy (FTIR), X-ray diffraction (XRD), Wettability, and Microhardness tests. The $ZnO_{4.10}/GO_{0.05}$ nanocomposite-modified coating exhibited exceptional corrosion protection by effectively enhancing charge transfer resistance and inhibiting coating failure.

Key Words : Epoxy, Graphene oxide, ZnO nanoparticles, Hybrid coating, Anti-corrosion coating.

Science Code : 91425

ÖZET

Yüksek Lisans Tezi

TUZLU ÇÖZELTİDE MAGNEZYUM ALAŞIMI İÇİN KOROZYON DİRENCİNE SAHİP GO/ZNO/EPOKSİ NANOKOMPOZİT KAPLAMANIN PERFORMANSI

Khaled ALJILOU

Karabük Üniversitesi
Lisansüstü Eğitim Enstitüsü
Makine Mühendisliği Bölümü

Tez Danışmanı:
Dr. Öğr. Üyesi Khaled M. N. CHAHROUR
Mayıs 2025, 75 sayfa

Bu çalışma, epoksi reçine kaplamalarda korozyon önleyici performansın artırılmasını, ZnO nanoparçacıklarının eklenmesi ve bu parçacıkların grafen oksit (GO) ile modifikasyonu yoluyla araştırmaktadır. Epoksi matrisi içerisinde etkin bir bariyer oluşturmak amacıyla, farklı ZnO ve GO ağırlık yüzdeleri optimize edilerek ZnO/GO nanokompoziti geliştirilmiştir. En belirgin iyileşme, %4.10 ZnO ve %0.05 GO içeren $ZnO_{4.1}/GO_{0.05}$ kaplamasında gözlemlenmiş; bu formülasyon 4.170 mmpy'lik düşük bir korozyon hızı (CR) ve 499020 Ω·cm⁻²'lik yüksek bir yük transfer direnci (R_{ct}) elde etmiştir. Bu değerler, yalnızca ZnO nanoparçacıklarıyla modifiye edilmiş kaplamalara (CR: 43.54 mmpy, R_{ct}: 129000 Ω·cm⁻²) ve saf epoksi kaplamalara (CR: 854.4 mmpy, R_{ct}: 54232 Ω·cm⁻²) kıyasla oldukça yüksektir. ZnO4.10/GO0.05 kaplamasının korozyon direnci, 3.5% NaCl çözeltisinde 72 saatlik daldırma sonrası gerçekleştirilen testlerle daha da doğrulanmış ve diğer

formülasyonlara göre üstün bozunma direnci sergilemiştir. Hazırlanan kaplamaların morfolojik, yapısal, termal ve yüzey özellikleri; Alan Emisyonlu Taramalı Elektron Mikroskobu (FESEM) ve enerji dağılımlı X-ışını spektroskopisi (EDX), Termogravimetrik Analiz (TGA), Fourier Dönüşümlü Kızılötesi Spektroskopisi (FTIR), X-ışını Difraksiyonu (XRD), Islanabilirlik ve Mikrosertlik testleri ile karakterize edilmiştir. $ZnO_{4.1}/GO_{0.05}$ nanokompozit ile modifiye edilen kaplama, yük transfer direncini etkili bir şekilde artırarak ve kaplama bozulmasını engelleyerek üstün korozyon koruma performansı sergilemiştir.

Anahtar Sözcükler : Epoksi, Grafen oksit, ZnO nanoparçacıkları, Hibrit kaplama, Korozyon önleyici kaplama

Bilim Kodu : 91425

ACKNOWLEDGEMENT

First and foremost, I would like to express my sincere gratitude to my advisor, Assist. Prof. Dr. Khaled. M. N. CHAHROUR, for their continuous support, valuable guidance, and encouragement throughout the course of my research and thesis writing.

I also gratefully acknowledge the financial support provided by the scientific research projects coordination unit (BAP), Karabük University, under the research grant KBÜBAP-23-YL-148, which made this study possible.

My deepest thanks go to my family for their endless love, patience, and motivation throughout this journey. Finally, I would like to thank all colleagues, friends, and individuals who contributed to this work in any way.

CONTENTS

Page

Page

Page

LIST OF FIGURES

Page

Page

LIST OF TABLES

Page

SYMBOLS AND ABBREVITIONS INDEX

SYMBOLS

ZnO	: Zinc Oxide
GO	: Graphene Oxide
Ep	: Epoxy Resin
MgAZ61	: Magnesium Alloy AZ61
NaCL	: Sodium Chloride
wt%	: Weight Percentage
AlMn	: Aluminum-Manganese Alloy
Mg_2Pb	: Magnesium Lead Intermetallic Compound
$Mg_{12}Nd$	: Magnesium Neodymium Intermetallic Compound
$Mg(OH_2)$	: Magnesium Hydroxide
OH^-	: Hydroxide Ion
MgO	: Magnesium Oxide
$MgCO_3$	: Magnesium Carbonate
Mg^{2+}	: Magnesium Ion
$MgCl_2$	: Magnesium Chloride
MgAZ31	: Magnesium Alloy AZ31
MgAZ80	: Magnesium Alloy AZ80
MgAZ91D	: Magnesium Alloy AZ91D
Al	: Aluminum
Cd	: Cadmium
Sn	: Tin
A3 steel	: Carbon Steel A3
316L stainless steel	: 316L Grade Stainless Steel
H62 Brass	: H62 Copper-Zinc Alloy (Brass)
LY12 Aluminum	: LY12 Aluminum Alloy (similar to 2024)
$Mg_{17}Al_{12}$	: Magnesium-Aluminum Intermetallic Compound

AlMnFe	: Aluminum-Manganese-Iron Compound
Mg_2Cu	: Magnesium Copper Intermetallic Compound
MgAM60	: Magnesium Alloy AM60
MgWE43	: Magnesium Rare-Earth Alloy WE43
AZ80-T5	: Magnesium Alloy AZ80 in T5 Temper
AE81 alloy	: Magnesium Alloy AE81
MgAZ91E-T6	: Magnesium Alloy AZ91E in T6 Temper
Al_2O_3	: Aluminum Oxide
SO_2	: Silicon Dioxide
pH	: Potential of Hydrogen
Si-O-C	: Silicon-Oxygen-Carbon Bond
Al AA2024	: Aluminum Alloy AA2024
APS	: Aminopropyltriethoxysilane
PET	: Polyethylene Terephthalate
O/O	: Organic/Organic composite
O/I	: Organic/Inorganic composite
I/I	: Inorganic/Inorganic composite
I/O	: Inorganic/Organic composite
CNTs	: Carbon Nanotubes
PTFE	: Polytetrafluoroethylene
PANI	: Polyaniline
I_{corr}	: Corrosion Current Density
E_{corr}	: Corrosion Potential
CR	: Corrosion Rate
K	: Constant (unit-dependent conversion factor)
V	: Voltage
A/cm^2	: Ampere per Square Centimeter
EW	: Equivalent Weight
P	: Density
g/equiv	: Gram per Equivalent
g/cm^3	: Gram per Cubic Centimeter
mmpy	: Millimeters per Year
TiO_2	: Titanium Dioxide

Hz	: Hertz
R_{ct}	: Charge Transfer Resistance
R_c	: Coating Resistance
R_s	: Solution Resistance
CPE_c	: Constant Phase Element of Coating
CPE_{dl}	: Constant Phase Element of Double Layer
C_2H_5OH	: Ethanol
M	: Molarity
mL	: Milliliter
rpm	: Revolutions Per Minute
°C	: Temperature
Z'	: Real Impedance Component
Z"	: Imaginary Impedance Component
Ω	: Ohm
F	: Frequency
C-H	: Carbon-Hydrogen Bond
C-O-C	: Ether Functional Group
C=C	: Carbon-Carbon Double Bond
HV	: Vickers Hardness

ABBREVITIONS

FESEM	: Field Emission Scanning Electron Microscopy
FTIR	: Fourier Transform Infrared Spectroscopy
XRD	: X-ray Diffraction
TGA	: Thermogravimetric Analysis
UV	: Ultraviolet
IGC	: Intergranular Corrosion
SCC	: Stress Corrosion Cracking
WE	: Working Electrode
RE	: Reference Electrode
CE	: Counter Electrode
OCP	: Open Circuit Potential
NPS	: Nanoparticles
EIS	: Electrochemical Impedance Spectroscopy

CHAPTER 1

INTRODUCTION

1.1. BACKGROUND

Most economically and safety-related concerns involving magnesium alloys are related to material degradation, with global estimated corrosion costs running into billions of dollars annually for industries worldwide. This shows the ever-increasing need to seek good protective solutions for certain industrial sectors, like maritime and chemical processing, which are highly corrosive. While generally considered among the best-performing protective coatings, epoxy suffers from progressive degradation in service performance, especially in seawater, leading to loss of surface integrity and eventual structural failure.

Epoxy has been widely used as a coating material to protect the various alloys [1,2] because of its outstanding processability, excellent chemical resistance, good electrical insulating properties, and strong adhesion/affinity to heterogeneous materials. Epoxy coatings generally reduce the corrosion of a metallic substrate subject to an electrolyte in two ways. First, they act as a physical barrier layer to control the ingress of deleterious species. Second, they can serve as a reservoir for corrosion inhibitors to aid the metal in resisting attack by aggressive species such as chloride anions. Nonetheless, the successful application of epoxy coatings is often hampered by their susceptibility to damage by surface abrasion and wear [3,4]. They also show poor resistance to the initiation and propagation of cracks [5]. Such processes introduce localized defects in the coating and impair their appearance and mechanical strength. The defects can also act as pathways, accelerating the entrance of water, oxygen, and aggressive species onto the metallic substrate, resulting in its localized corrosion. Furthermore, being hydrophilic, epoxy coatings experience large volume shrinkage upon curing and can absorb water from the surroundings [6,7]. The

pores in the cured epoxy coating can assist in the migration of absorbed water and other species to the epoxy–metal interface, leading to the initiation of corrosion of the metallic substrate and the delamination of the coating.

Nanocomposite coatings are currently receiving great interest in material protection, especially for lightweight and corrosion-active metals such as magnesium alloy, due to their unique properties originating from nanoscale structures. These coatings form compact and homogeneous layers that serve as highly effective barriers against corrosive agents such as moisture, oxygen, and salts, substantially enhancing the corrosion resistance of the substrate. The fillers at the nanoscale used in such coatings include, among others, silica, graphene, graphene oxide, and metal oxides. In addition to providing impermeability, these nano-fillers help to enhance mechanical strength and toughness. These properties make the substrate more resistant to wear, scratches, and other mechanical stresses, while guaranteeing good adhesion between the coating and the base material.

1.2. RESEARCH PROBLEM

The current study aims to overcome the weaknesses of traditional epoxy coatings, which are susceptible to water and ion penetration, by incorporating ZnO nanoparticles into the epoxy matrix. Various studies have proved that incorporating nanoparticles significantly enhances the protective performance of coatings by creating a denser and less permeable barrier against corrosive agents. However, the interactions between nanoparticles, the epoxy matrix, and magnesium alloy substrates under varying environmental conditions remain poorly understood. The adhesive strength between the coating and substrate is critical in maintaining long-term protective effectiveness. Adhesion failure can lead to layer delamination, negatively impacting the coating's protective ability and reducing its overall durability. This work aims to develop hybrid coatings based on epoxy resin, zinc oxide (ZnO) nanoparticles, and graphene oxide (GO) nanoparticles, and investigate their performance in Magnesium alloy surfaces. A key focus of the research is the corrosion resistance and mechanical strength assessment of the epoxy/ZnO and epoxy/ZnO/GO coatings compared to conventional epoxy coatings. This can be achieved by improving the corrosion performance of

epoxy coatings with ZnO nanoparticles designed for severe environmental exposure in a range of demanding industries, such as chemical, marine, and more. By investigating the structural and morphological properties of the nanocomposite, this study seeks to deepen our understanding of the interactions between graphene oxide (GO), ZnO nanoparticles, the epoxy matrix, and the Magnesium alloy substrate. Tests will be conducted to evaluate the coating's adhesion strength, corrosion resistance in saline conditions, and mechanical properties such as microhardness.

1.3. AIM OF THE RESEARCH

This research aims to develop and improve nanocomposite coatings based on epoxy, ZnO nanoparticles, and graphene oxide (GO) nanoparticles to enhance the corrosion resistance, mechanical performance, and thermal stability of MgAZ61 alloy substrates. This study seeks to comprehensively understand how these coatings perform under various conditions and establish their potential for practical applications in industries requiring lightweight and corrosion resistant materials. The structural and morphological properties of the nanocomposite will be investigated to understand how the incorporating of ZnO nanoparticles in the epoxy resin enhance the corrosion resistance, furthermore the incorporation of GO nanoparticles in epoxy/ZnO. This study is intended to enhance corrosion resistance, and the mechanical properties of MgAZ61 alloyes.

1.4. OBJECTIVES OF THE STUDY

1. To synthesize corrosion-resistant zinc oxide (ZnO) nanoparticles and epoxy resin coating with varying weight percentages of ZnO.
2. To incorporate graphene oxide (GO) as a modification layer to enhance the corrosion resistance and mechanical properties of epoxy/ZnO nanocomposite coatings.
3. To examine the corrosion protection performance of the prepared coatings using electrochemical potentiodynamic polarization and impedance spectroscopy.

4. To evaluate the characterization of prepared nanocomposite coatings by applying Thermal Gravimetric Analysis (TGA), Fourier Transform Infrared Spectroscopy (FTIR), Scanning Electron Microscopy (SEM), and microhardness test.

1.5. SIGNIFICANCE OF THE RESEARCH

This study is important because it can contribute to coating and corrosion protection technologies essential in industrial environments where magnesium alloy is common. Some industries heavily dependent on magnesium alloy construction include the building, energy, and transportation sectors. Better corrosion prevention methods must be developed as the cost of maintaining and repairing damaged infrastructure is very high.

1.6. SCOPE AND LIMITATIONS

This research elaborates and characterizes nanocomposite coatings based on epoxy, ZnO nanoparticles, and graphene oxide to protect MgAZ61 alloy substrates. The experimental work involved synthesizing a few wt% of ZnO and GO coatings in an epoxy matrix via a spin-coating technique. The characterizations will be made through structural, morphological, and thermal analysis by FESEM, FTIR, XRD, and TGA techniques, together with determining some mechanical properties, like microhardness and surface wettability. Electrochemical performance will be investigated by EIS and Tafel polarization tests in a corrosive environment simulated to find the optimum composition for maximum corrosion resistance, mechanical robustness, and thermal stability.

Some limitations to the research include that experimental conditions will be limited to a controlled laboratory environment using a 3,5% NaCl solution, possibly not accurately mimicking corrosive environmental elements. The thermal stability tests are limited to the temperature utilized in TGA and may not reflect extreme conditions. Besides, the coating technique used, namely spin coating, may not directly apply to other coating techniques applied in industries, such as spray or dip coating. This study

does not consider long-term durability and performance under cyclic environmental stresses, including temperature fluctuations and UV exposure. Despite these limitations, the study gives relevant insights and a starting point for further investigation and optimization of nanocomposite coatings for industrial applications.

CHAPTER 2

THEORETICAL STUDY

2.1. CORROSION OF MAGNESIUM ALLOY

Corrosion behavior of magnesium alloys, which are lightweight materials widely considered for automotive, aerospace, and electronics applications. Magnesium alloys face significant challenges despite their potential due to their susceptibility to corrosion. This vulnerability emanates fundamentally from the imperfections in the oxide films and galvanic effects because of impurities and secondary phases, such as AlMn [8], Mg_2Pb [9], and $Mg_{12}Nd$ [10].

Several factors influence the corrosion behavior of magnesium alloys. Metallurgical characteristics include alloy composition, microstructure, and grain size [11]. For instance, while a higher aluminum content improves overall corrosion resistance, too high an optimum level may have negative effects. [9]. Heat treatment and welding are process treatments that affect corrosion resistance through their impact on microstructure and secondary phase distribution. Environmental conditions, such as pH, humidity, temperature, and chloride ion concentration, also impact this resistance by accelerating the rate of degradation.

The article points out that the precise mechanisms of magnesium alloy corrosion are still unclear, which indicates research gaps. Particularly, the effects of welding technologies and environmental conditions on corrosion should be researched. Moreover, it is urgently needed to develop innovative coating technologies that meet the diverse requirements of modern applications [11].

The corrosion behavior of magnesium (MgAZ61) alloys is affected by factors such as the composition of the alloy and microstructure [12,13]. The properties of the

surface film formed in the medium to which they are exposed [14]. Regarding the latter, there has been a lot of work on the development of corrosion product layers that precipitate on the surface of magnesium and its alloys when exposed to saline solutions [15-17]. It is known that the surface layer of corrosion products formed in saline environments consists primarily of brucite $Mg(OH)_2$. since magnesium dissolution promotes the production of hydroxide ions (OH^-) via the cathodic reaction [18-20]. The surface film structure has been described variously as a mixed $MgO/Mg(OH)_2$ layer [21, 22], or a bilayer of an inner MgO layer and an outer $Mg(OH)_2$ layer [17,23]. Additionally, studies of Mg alloys under ambient atmospheric conditions have detected Mg-carbonate ($MgCO_3$) in the outer layer of the corrosion film [17,21,22,24].

During Mg dissolution, Mg^{2+} ions migrate to the surface and react with OH^- ions, forming a porous $Mg(OH)_2$ layer over the inner MgO barrier film [25]. In contact with a NaCl solution, chloride ions adsorbed on the magnesium alloy surface convert Mg $(OH)_2$ into soluble $MgCl_2$ [26,27], which exposes new areas of unprotected magnesium to further corrosion.

In previous studies, it has been observed that the chemical composition of the corrosion product layer, whether formed during atmospheric exposure [20] or under high-humidity conditions [21], [26]Influencing the subsequent corrosion behavior of Mg alloys, advanced surface elemental composition analyses revealed significant differences in the surface chemistry of the corrosion product layers formed on commercially pure Mg, AZ31, AZ80, and AZ91D alloys stored at room temperature. A correlation between surface elemental composition results and gravimetric measurements demonstrated that lower corrosion rates were associated with a higher proportion of magnesium carbonate on the surface [22].

2.2. CORROSION TYPES

Magnesium alloys are very susceptible to galvanic corrosion, which can be caused by heavy metal contamination exceeding the limits, flux residues, and poor design and assembly practices. Iron, nickel, and copper, having low hydrogen overvoltage, can serve as efficient cathodes and cause severe galvanic corrosion. In contrast, metals

such as aluminum (Al), zinc (Zn), cadmium (Cd), and tin (Sn) have an active corrosion potential coupled with high hydrogen overvoltage and are considerably less damaging.

Galvanic corrosion generally assumes the form of general corrosion, especially around the substrate where it interfaces with inner secondary phases. A study focused on the galvanic activity of AZ91D, AM50, and AM60 cast magnesium alloys coupled with A3 steel, 316L stainless steel, H62 brass, and LY12 aluminum alloy under atmospheric exposure conditions [11]. The results showed that all the magnesium alloys act as anodes, and their corrosion rate increases when coupled with the abovementioned metals.

Even high-purity magnesium alloys are not immune to galvanic corrosion when coupled with other metals. However, the risk can be mitigated through careful material selection, improved design, and the strategic use of coatings and insulating materials. For instance, using aluminum fasteners from the 6000 series has significantly reduced galvanic corrosion of magnesium alloys in salt spray environments [28].

2.2.1. Pitting Corrosion

Magnesium is naturally a passive metal; however, pitting corrosion can occur at its free corrosion potential when exposed to chloride ions in a non-oxidizing medium [29]. Corrosion pits are typically observed to initiate defects near secondary phase particles, such as $Mg_{17}Al_{12}$ and AlMn, due to the breakdown of the passive layer [8], [29]. This process forms an electrolytic cell: the secondary phase particles (e.g., AlMn, AlMnFe, $Mg_{17}Al_{12}$, and Mg2Cu act as cathodes, while the surrounding magnesium matrix acts as an anode.

For example, when as-extruded AM60 magnesium alloy was immersed in a natural 3.5% NaCl solution, corrosion pits were observed around the AlMn particles, indicating that these particles are the initiation sites of localized corrosion.

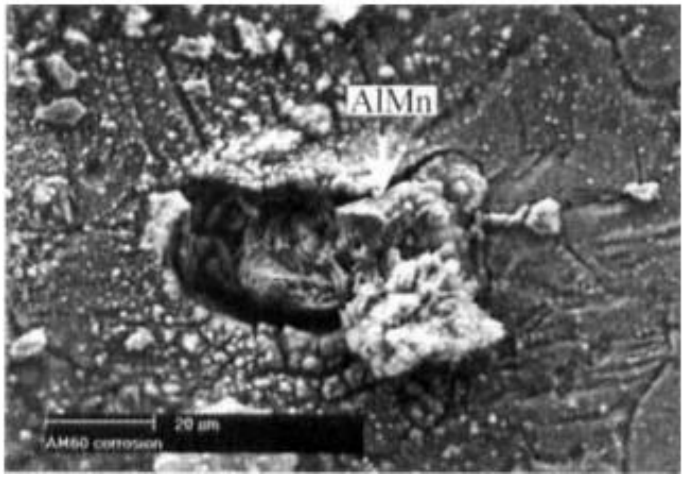

Figure 2.1. Pitting morphology of extruded AM60 in 3.5%NaC1 aqueous solution [30].

2.2.2. Intergranular Corrosion IGC

IGC occurs along grain boundaries due to the precipitation of secondary phases, as these boundaries are preferred sites for precipitation and segregation in alloys. Generally, alloys containing intermetallic phases or compounds are considered highly susceptible to intergranular corrosion. However, some debate has been on whether magnesium alloys experience true IGC.

On the other hand, recent studies show that magnesium alloys suffer from intergranular corrosion. For example, research found that WE43 magnesium alloy exhibited a preferential attack at grain boundaries when exposed to a 3.5% NaCl solution [31]. Another research pointed out that during an initial period of immersion in mild corrosive media, localized attack occurs at grain boundaries associated with cathodic precipitates and, therefore, can be defined as intergranular (or intercrystallite) corrosion [32].

One example of IGC is found in the AE81 alloy, where areas with lower aluminum concentrations corroded more rapidly than areas rich in aluminum. Intergranular corrosion was also recorded for the aged AZ80 magnesium alloy after immersion in 3.5% NaCl solution for 1 hour. The corrosion in this case advanced along the grain boundaries, forming deep and narrow paths.

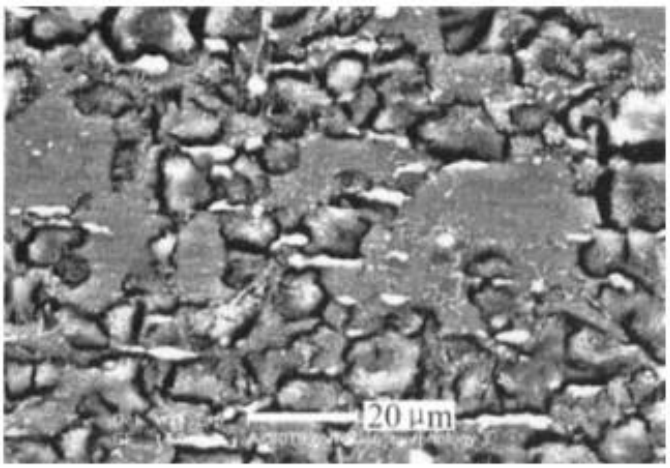

Figure 2.2. Intergranular corrosion morphology of AZ80-T5 in 3.5%NaCI aqueous solution after 1 h.

2.2.3. Filiform Corrosion

Filiform corrosion normally appears on metal surfaces such as steel, aluminum alloys, and magnesium alloys. The corrosion is caused by active galvanic cells across the metal surface, where the head acts as the anode while the tail acts as the cathode. Filiform corrosion normally relates to the metal surface with an applied protective coating. It does not occur on bare, pure magnesium [33].

In the studies on AZ91 magnesium alloy, researchers found that the early stages of its corrosion are dominated by both pitting and filiform modes of corrosion. Filiform corrosion often starts corrosion pits on the surface [34].

2.2.4. Crevice Corrosion

It has been claimed that magnesium alloys do not undergo true crevice corrosion [12,35]. While corrosion in narrow gaps, or "crevices", may seem to resemble crevice corrosion, it is not technically the same. The observed corrosion in such areas is primarily caused by moisture retention within the crevice, which promotes localized metal corrosion over extended periods due to its inability to evaporate.

Filiform corrosion is a special form of crevice corrosion. Given that filiform corrosion may occur on magnesium alloys, it could be assumed that crevice corrosion could also occur under these conditions. A study suggested that crevice corrosion of magnesium and its alloys may be initiated through a hydrolysis reaction, especially in an environment in which oxygen does not play a significant role in the corrosion mechanism [32]. In such cases, the formation of magnesium hydroxide might affect the interface properties between the magnesium surface and the solution trapped inside the crevice.

2.2.5. Stress Corrosion Cracking SCC

Stress corrosion cracking (SCC) is an extremely dangerous kind of corrosion damage that greatly influences the efficiency of engineering equipment, vessels, and other structures. Much research on SCC in magnesium alloys has been conducted on extruded or rolled alloys. Two primary mechanisms generally explain SCC in Mg alloys. The first involves continuous crack propagation driven by anodic dissolution at the crack tip. The second mechanism is characterized by discontinuous crack propagation, occurring through a sequence of mechanical fractures initiated at the crack tip [36].

2.2.6. Corrosion Fatigue

In recent years, a great amount of fatigue data on magnesium alloys has been accumulated [37]. Most of the experimental studies have been related to fatigue life. Magnesium alloys exhibit an endurance limit if tested in air, and a decrease in grain size reduces fatigue strength. Resistance to fatigue crack propagation follows the reverse trend: it decreases with a reduction in grain size [38]. Numerous experimental studies have demonstrated a significant reduction in fatigue strength or fatigue life in sodium chloride solutions, as well as in tap water or distilled water [37]. For example, the corrosion fatigue resistance of AZ91E-T6 magnesium alloy was significantly lower in 3.5% salt water compared to its performance in air [39]. Moreover, the effects of corrosive environments on the fatigue life of extruded magnesium alloys are more pronounced than in die-cast magnesium alloys [38].

2.3. CORROSION PROTECTION MECHANISMS

Corrosion protection mechanisms are critical in protecting metallic substrates, especially in hostile environments. It has been proved that inhibitors, nanofillers, nanocontainers, and surficial protective coatings efficiently enhance material corrosion resistance.

2.3.1. Inhibitors

Inhibitors are chemical substances that decrease the corrosion rate either by forming a protective film on the material's surface or by changing the corrosive environment. For example, anodic inhibitors retard the oxidation reactions, whereas cathodic inhibitors decrease the reduction processes. Mixed inhibitors, which combine both effects, have also been reported to be successful in several works. A study emphasized that organic inhibitors could create adsorption layers on metallic substrates, which may drastically reduce the corrosion rate. The addition of inhibitors to epoxy-based coatings is a well-known approach to improve their chemical resistance and durability [40].

2.3.2. Nanofillers

Nanofillers such as ZnO, Al_2O_3, SiO_2, and graphene oxide have been added to coatings to enhance their mechanical and barrier properties. Nanofillers act by creating tortuous diffusion paths, which delay the penetration of corrosive species. Many articles reported that the addition of graphene oxide to epoxy coatings significantly enhanced corrosion resistance due to the high aspect ratio and impermeability of GO [41]. Researchers also reported that the addition of ZnO nanoparticles enhanced structural strength and resisted corrosion in nanocomposites [42].

2.3.3. Nanocontainers

Nanocontainers represent advanced systems of controlled encapsulation-release by an environmental stimulus, either in the form of critical pH or mechanical damage. An

study extensively took advantage of such nanocontainers for embedding corrosion inhibitors, thus providing them with self-healing ability in coatings [43]. These systems could protect inhibitors from release at just that moment when the beginning of corrosion occurs, which creates the maximum conditions for their action, and hence prolongs the time of service of the coating.

2.3.4. Surficial Protective Coatings

Act as a physical barrier, separating the substrate from the aggressive environment. Epoxy-based coatings have been widely investigated owing to their good adhesion and chemical resistance. A study on the anticorrosion performance of the epoxy–polyamide nanocomposites containing ZnO nanoparticles [44]. Additionally, hybrid nanocomposite systems have been explored, demonstrating synergistic effects that combine the structural, mechanical, and electrochemical benefits of nanomaterials [45]

2.4. TYPES OF COATING

2.4.1. Inorganic Coatings

Generally, the inorganic components significantly contribute to the improvement in the performance of the sol-gel hybrid coatings, which is related to enhancement in adhesion and corrosion resistance, as well as in the mechanical properties of coatings. Inorganic sols primarily enhance the adhesion between metals and hybrid coatings, act as adhesion promoters in metal pre-treatment, and improve overall polymer performance in hybrid coatings. Conventional polymer coating systems are mechanically flexible and tough but often lack abrasion and thermal resistance. Due to their low oxygen diffusion and excellent mechanical properties, inorganic sols overcome these deficiencies by creating a strong adhesion layer between metallic substrates and organic coatings. Investigations have proved that silica-polymer hybrid film coatings greatly improve the corrosion resistance of materials like stainless steel and zinc-plated steel.

Further enhancements include inorganic sol incorporation into polymers such as PMMA, enhancing adhesion strength and thereby anticorrosion efficiency [46]. The mechanical properties, such as hardness and abrasion resistance, are improved for sol-gel/epoxy resin hybrids. These also offer excellent anti-corrosion performance even without conventional inhibitors such as hexavalent chromates. Hybrid coatings prepared from alkyd resins and sol-gel precursors present an improved heat resistance owing to the formation of Si–O–C bonds, although the curing may be slower because of interactions with driers [47].

The species and density of functional groups within the sol particles significantly affect the anticorrosion properties of hybrid coatings. Research has shown that the performance of sol-gel coatings is related to their composition, synthesis methods, and processing relationships. For instance, titanium tetrapropoxide and acetylacetone coatings on AA2024 aluminum alloys have shown optimum protection in chloride environments. Incorporating inorganic sols into hybrid coatings generally enhances adhesion, mechanical properties, and corrosion resistance, thus making them effective in various industrial applications. [48].

2.4.2. Organic Coatings

Incorporating organic groups or polymers in inorganic sol-gel coatings will effectively avoid the intrinsic deficiencies of pure inorganic coatings when used for corrosion-resistant coatings. Among the shortcomings in pure inorganic coatings developed by sol-gel processing, the following may be stated: difficulty in obtaining thick coatings without cracking, brittleness with high crack-forming potential [47], and the presence of apertures in the film [49]. These limitations lead to unsatisfactory physical barrier properties, making them unsuitable for effective corrosion protection. Two main routes normally introduce the organic components in inorganic coatings: one is defect healing, and the other is incorporation of organic components into the sol–gel matrix. Defect healing consists of treating inorganic coatings with appropriate organic alkoxysilanes, reducing the permeability of the inorganic layer by healing defects. This approach is often used in hybrid coatings containing low organic content or in the defective healing of inorganic films. As a specific example, the oxygen transmission

rate—a function of permeability of a hybrid coating on poly (ethylene terephthalate) film is greatly improved by overcoating a thin layer of oligomerized amino-silane (APS) onto a silica (SiO_2) coating. Tests have shown that defects of APS on a 48 nm thick SiO_2 layer reduce macro-defects and nano-defects to cause a two-order-of-magnitude to decrease in oxygen permeability [50]. Similarly, a solution of 1 wt% amino silane applied to SiO_2-coated PET films halves the permeability of the resulting silane–silica hybrid coating compared to an as-deposited SiO_2-coated PET film [47].

The corrosion resistance and overall performance of hybrid coatings are greatly related to the ratio between the inorganic and organic components in the sol-gel matrix. The organic component adds not only to the reduction of porosity and increase in density of the coating but also allows the realization of thicker coatings and reduces the curing temperature. Such properties, when combined, make hybrid coatings more efficient as corrosion-resistant layers, with flexibility and toughness for superior protection in varied applications. The interplay between organic and inorganic components in hybrid coatings thus represents an important step toward overcoming the limitations of traditional inorganic sol-gel films.

2.5. EPOXY COATING

Epoxy coating is an extremely durable, versatile, and aesthetically appealing surface treatment used in several residential, commercial, industrial, and marine applications. Mixing epoxy resin with a hardener creates a durable, cohesive protective coating that is resistant to corrosion, chemicals, and water. It's perfect for application on garage floors, warehouses, laboratories, and aesthetic spaces like showrooms. Its surface is easy to clean and maintain, stain-resistant, and spill-resistant, and can last decades if properly maintained.

Overall, epoxy coating is versatile and reliable for surface enhancement and protection in diverse environments. The ability of the material to combine functionality, durability, and style has made it a preferred option when long-lasting and aesthetically pleasing surface treatment is desired.

2.6. NANOCOMPOSITE-POLYMER MATRIX COATINGS

The addition of nanofillers and reinforcements at the nanoscale level has significantly enhanced the properties of the composites due to an improved interface and better load transfer. Nanofillers combine the advantages of epoxy and nanomaterials, giving rise to a new class of materials called epoxy nanocomposites, a new field of research for enriching the mechanical properties of polymeric matrix composites. Unlike traditional fillers, nanofillers require only a small amount of material to achieve significant property enhancements and thus are ideal for applications in aerospace and other high-performance industries. The enhancement includes strength in flexural, tensile, impact, and interlaminar shear tests, improving the glass transition temperature.

Traditionally, the major contribution to research on nanomaterials-reinforced polymer composites for structural applications has come from isotropic spherical nanomaterials. Large quantities of nanomaterials with high-aspect ratios, such as clays, graphene, and nanotubes, have recently been considered very interesting due to their highly elongated geometries, which give composites anisotropic properties. This anisotropy, combined with increased interfacial areas by nanofillers considerably influences epoxy nanocomposites' mechanical, thermal, electrical, and chemical properties. Unlike microfilters, nanofillers create larger interfaces due to their high surface-to-volume ratio of the constituting atoms or molecules, leading to improved thermal, mechanical, electronic, and chemical performance.

Nanocomposite coatings are materials comprising at least two immiscible phases separated by an interface region, with at least one dimension at the nanometer scale. The main component, the matrix, acts as the host material where fillers are dispersed [51]. These coatings are classified based on either the type of nanostructured fillers or the type of matrix. These nanostructured fillers can be divided into three main groups: 0D nanocomposite coatings with fillers having nanoparticles with all dimensions in the nanoscale, and 1D nanocomposite coatings having fillers of nanotubes or whiskers with two dimensions in the nanoscale [51]. Matrices can be classified into organic and inorganic, so generally, there are four big classes of nanocomposite coatings:

organic/inorganic (O/I), organic/organic (O/O), inorganic/organic (I/O), and inorganic/inorganic (I/I) coatings.

2.6.1. Materials

The materials used for the matrix vary considerably. Organic matrices, known under popular names polymer-based nanocomposites, include but are not limited to the following set of polymers: epoxy [52,53], polyurethane [54,55]. Nanofillers of such coatings represent a gigantic class of materials. Inorganic nanofillers include carbides [56], nitrides [57], borides [58], and carbon nanotubes (CNTs) [59]. The most used organic nanofillers include PTFE [60], PANi [61], and cellulose-based materials such as nanocellulose and cellulose nanocrystals [62,63].

2.6.2. Preparation Method

Among the many preparation methods, the sol-gel technique is outstanding for producing high-quality films of millimicron-scale thickness. It also represents a complementary technique to physical depositions; however, the technique does suffer from certain disadvantages, which include crack formation by tensile stresses during drying, besides limitations in maximum film thickness. In the case of inorganic matrices, the second-phase nanofillers can be introduced during the process of sol-gel to produce I/I coatings [64]. Organic matrices, on the other hand, are usually treated by the sol-gel technique in order to produce inorganic nanophases within the organic matrix [62]. Among common precursors are silicon, titanium, aluminum, and zirconium metal alkoxides. Silanes and organic molecules can form coatings with silica nanoparticles or nanophases under controlled conditions. In such materials, organic and inorganic phases are usually coupled by coupling agents to achieve proper mechanical and thermal properties.

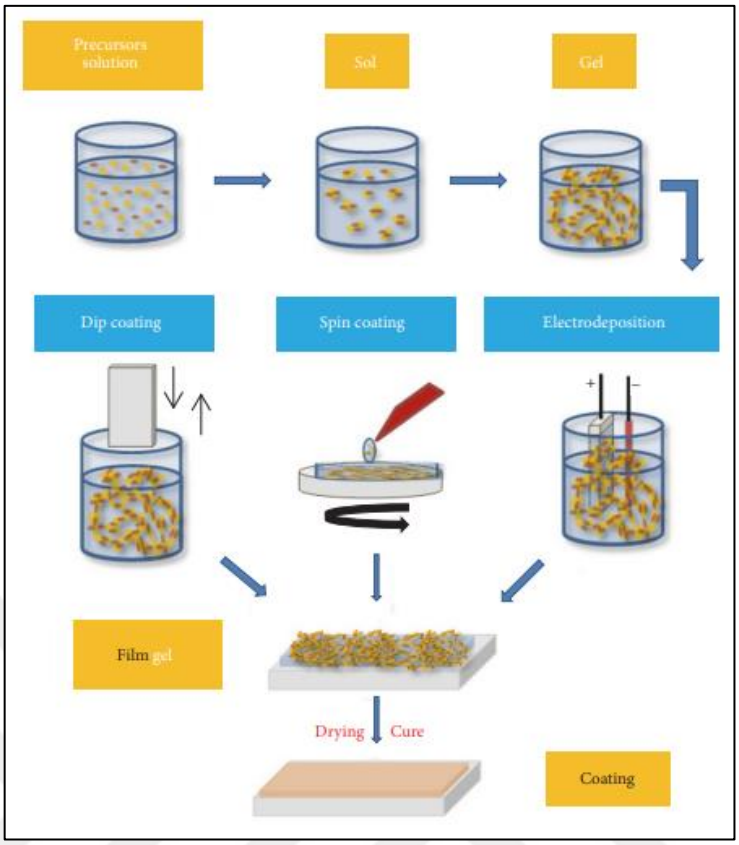

Figure 2.3. Preparation of coatings by sol-gel method [65].

2.7. TECHNIQUES FOR DISPERSION PROCESSING OF NANOCOMPOSITES IN EPOXY

2.7.1. Method of Dispersion Via Ultrasonication

Ultrasonication is the most effective and widely used technique for the dispersion of nanoparticles in the epoxy matrix to prepare nanocomposites. Ultrasonication generates high-frequency sound waves, inducing acoustic cavitation, a process related to microbubbles' rapid formation and collapse in a liquid medium. This releases tremendous energy and produces strong shear forces that can break up the agglomerated nanoparticles and ensure their uniform dispersion in the epoxy resin.

The epoxy matrix is mixed with nanoparticles and then treated with ultrasonic waves for a certain period. Ultrasonication helps to overcome the van der Waals forces, which often result in the clustering of nanoparticles, hence promoting better dispersion and

homogeneity of the mixture. Homogeneity in dispersion is a crucial factor to obtain the best mechanical, thermal, and electrochemical properties of the resulting nanocomposite.

For such an ultrasonication process, there is a real need for optimum parameters like amplitude, frequency, and time to prevent overheating and/or epoxy matrix degradation. Normally, solvents like ethanol are used to facilitate preliminary dispersions of nanoparticles before mixing with epoxy resin. This technique finds applications for various high-performance nanocomposites to improve filler distribution and interfacial bonding among the nanoparticles and the matrix.

2.7.2. Mixing Dispersion Via Mechanical Method

Mechanical stirring is one of the common techniques used in the dispersion of nanoparticles into the epoxy matrix to produce nanocomposites. It employs a magnetic or mechanical stirrer to mix the nanoparticles with the epoxy resin under controlled conditions. Stirring will introduce shear forces that will result in the distribution of nanoparticles within the matrix, leading to homogeneous dispersion.

In this process, the nanoparticles are generally pre-dispersed in a solvent, such as ethanol, which assists in their preliminary distribution. The resultant mixture of solvent and nanoparticle is added to the epoxy resin and stirred for a certain period to ensure that the nanoparticles are incorporated into the resin. The speeds of mixing, stirring time, and temperature of the processes are carefully monitored to avoid settling or any agglomeration of nanoparticles.

Although mechanical stirring might not disperse some kinds of nanoparticles as well as ultrasonication, it represents a highly effective and simple way of preliminary mixing. Very often, it is combined with other techniques, such as ultrasonication, to get better dispersion to improve the properties of the nanocomposite. Adequate mixing by mechanical means ensures homogeneity of the matrix, which is especially important for attaining proper mechanical, thermal, and electrochemical performance of the final nanocomposite coating.

2.8. ELECTROCHEMICAL CORROSION TESTING METHODS

Electrochemical techniques are substantial in assessing the corrosion resistance of protective coatings. Among these, the Tafel polarization and Electrochemical Impedance Spectroscopy (EIS) methods are extensively employed to evaluate the performance of coatings like epoxy composites and nanocomposites.

2.8.1. Tefal Technique (Tefal Curves Analysis)

The Tafel polarization method is a potentiodynamic technique that measures the corrosion behavior of materials by recording the current response to a range of applied potentials. Extrapolating the linear portions of the anodic and cathodic branches of the polarization curve can determine the corrosion current density (I_{corr}) and corrosion potential (E_{corr}). These parameters are instrumental in calculating the corrosion rate using Faraday's law [66].

$$CR = \frac{K \cdot I_{corr} \cdot EW}{\rho} \quad (2.1)$$

1. K is a unit-dependent constant (e.g., 3.27×10^3 for mm/year when $\boldsymbol{I_{corr}}$ is in (A/cm²),
2. I_{corr} is the corrosion current density (A/cm²),
3. EW is the equivalent weight of the metal (g/equiv).
4. ρ is the density of the metal (g/cm³).

Recent studies have demonstrated the efficacy of this method in evaluating epoxy-based coatings. For instance, coatings containing graphene oxide (GO), Alumina (Al_2O_3), Zinc oxide (ZnO), and Titanium dioxide (TiO_2) nanoparticles have shown significant reductions in (I_{corr}), indicating enhanced corrosion resistance. These are attributed to the barrier properties brought by the nanofillers that resist corrosive species penetration.

2.8.2. EIS Technique (Nyquist and Bode Curves Analysis)

Electrochemical Impedance Spectroscopy (EIS) is a non-destructive technique used to characterize coatings' corrosion protection performance and barrier properties. EIS measurements are carried out by applying a small sinusoidal AC voltage (typically 5–10 mV) over a range of frequencies (from 100 kHz to 0.01 Hz) at the open-circuit potential.

The results are typically presented in the form of:

1. Nyquist plots, which show the imaginary vs. real impedance and are used to extract values like charge transfer resistance (R_{ct}) and coating resistance (R_c).
2. Bode plots, which show the variation of impedance magnitude and phase angle as a function of frequency.

CHAPTER 3

MATERIALS and EXPERIMENTAL METHODS

3.1. CHEMICALS

3.1.1. MgAZ61 Alloy Substrate

A magnesium/aluminum/zinc alloy was chosen as the substrate due to its lightweight nature, high strength to weight ratio, and excellent corrosion resistance properties. This alloy is widely used in aerospace, automotive, and marine industries, making it an ideal sample for testing the protective properties of nanocomposite coatings. The substrate was prepared by encasing it in a Teflon holder to ensure only the coated surface was exposed during testing. The Teflon casing not only provides electrical insulation but also protects the uncoated parts of the alloy during electrochemical studies. A small copper rod was inserted through a drilled hole at the back of the alloy to provide electrical connections for Electrochemical Impedance Spectroscopy (EIS) studies. The copper rod ensured a stable and cosistant electrical pathway while minimizing contact resistance during testing.

3.1.2. Ethanol (C_2H_5OH)

One dispersing solvent was purchased from Sigma Aldrich. Analytically pure ethanol with a ≥99.5% purity was used to achieve an evenly dispersed form of ZnO and GO within the epoxy matrix. The solvent was stored in well-closed bottles and handled under a well-ventilated working area to minimize evaporation and contamination.

3.1.3. Epoxy Resin and Hardener

Served as the matrix material, giving adhesion and strength to the coating. Araldite LY 556 resin was used, and the Aradur 2954 hardener was provided by Huntsman Corporation. These two are noted for their high performance in industrial applications, with the optimum ratio of resin to hardener available from the manufacturer for optimal crosslinking and curing.

3.1.4. Zinc Oxide (ZnO) Nanoparticles

ZnO nanoparticles were purchased from Nanografi Nano Technology, a reputable source of high-quality nanomaterials. The ZnO nanoparticles were 18 nm in particle size and ≥99.50% pure and played a critical role in enhancing corrosion resistance, mechanical, and thermal performance of the coating. The nanoparticles were stored in a dry location away from moisture to maintain their integrity.

3.1.5. Graphene Oxide (GO)

GO is added to ethanol/ZnO nanocomposite coatings to improve corrosion resistance, mechanical strength, thermal stability, and nanoparticle dispersion, creating a more compact and effective protective barrier on metal surfaces. GO was purchased from Nanografi Nano Technology, one of the well-known providers of high-quality graphene materials. The GO purchased was 0.5-1.3 nm for single layer, and purity >99.50%. The oxygen-functionalized layered structure allowed for dispersion in the epoxy matrix through the assistance of ethanol/ZnO as a solvent.

3.1.6. Sodium Chloride (NaCl)

Supplied by ITK Chemicals with a purity of ≥85%, it was used to prepare the electrolyte solution for the electrochemical cell, a critical component for EIS and Tafel testing. The 3.5% NaCl was dissolved in distilled water, which was prepared in-house using a laboratory-grade distillation apparatus and stored in clean, airtight containers

to prevent contamination. Distilled water was also used for cleaning during substrate preparation and electrochemical testing.

3.2. MATERIALS

In addition to the chemicals, specific equipment was essential for synthesis. A magnetic stirrer from Intllab, was used to achieve an initial homogeneous mix of the epoxy and fillers, with adjustable stirring speeds up to 1500 rpm. Following this, a Hielscher Ultrasonics UP400St ultrasonic device, capable of delivering 400 W of power, was utilized to break up agglomerates of ZnO and GO, ensuring uniform dispersion within the matrix.

Accurate weighing of all chemicals was performed using a Mettler Toledo ML-T series chemical balance, offering a precision of up to 0.001 g. The mixing and handling of chemicals were done in Pyrex glass breakers of 10 mL, 20 mL, and 40 mL capacities, chosen for their excellent resistance to thermal and chemical stress. The coating process involved the use of a Spin coater made by undergraduate students of Karabuk University Figure 3.5. The spin coater allowed us to produce uniform GO/ZnO/epoxy films with controlled thickness across all samples, ensuring consistent comparison in thermal and electrochemical tests

Figure 3.1. Spin coating device with maximum speed up to 1500 rpm

3.3. PREPARATION OF THE COATINGS

3.3.1. Cleaning The MgAZ61 Alloy: Grinding and Polishing

The cleaning process of the MgAZ61 alloy is critical to ensure a clean, smooth, and uniform surface for the coating. Proper surface preparation enhances the adhesion and performance of the applied coating.

3.3.2. Preparation of Chemicals and Materials in a Clean Environment

To ensure cleanliness and uniformity throughout the coating preparation process, all chemicals and materials were handled under controlled conditions within a well-ventilated clean room environment. The experimental work was conducted in a laboratory equipped with a fume hood to safely manage volatile substances such as ethanol and to minimize the risk of contamination. Prior to the commencement of any procedures, all laboratory surfaces were thoroughly cleaned using ethanol to eliminate dust and residues. Strict precautions were taken to maintain a dust-free workspace, and

all personnel involved adhered to standard laboratory safety protocols, including the use of gloves, lab coats, and protective eyewear. Analytical-grade ethanol was used as the dispersion solvent and was measured precisely into clean beakers of appropriate volumes (10 mL, 20 mL, and 40 mL) to ensure accurate formulation. The epoxy resin and hardener were weighed according to the manufacturer's specified ratio, transferred into clean container, and reserved for later mixing.

All apparatus used in the preparation and coating processes were handled with equal care to maintain experimental integrity. The ultrasonic device employed for dispersing ZnO and GO nanoparticles in ethanol was thoroughly cleaned with ethanol and calibrated to ensure consistent energy output throughout the dispersion process. The magnetic stirrer, utilized for mixing the epoxy resin, hardener, and nanoparticle dispersions, was similarly cleaned and fitted with a sterilized stir bar to avoid cross-contamination. Prior to coating, the spin coater designated for applying the formulation onto MgAZ61 alloy substrates was carefully inspected. Its platform was cleaned using ethanol to eliminate any residual contaminants.

3.3.3. Preparation of Pure Epoxy Coating Solution and Application Process

The first step of this study was the preparation and deposition of a neat epoxy coating onto the MgAZ61 alloy substrate. This was the reference point to compare the properties of the epoxy matrix without further modification. The preparation was carried out in a systematic way to obtain consistent coating.

The process began by making 12 mL of ethanol, measuring and placing it in a sterile glass tube. 20 mL of epoxy resin was added slowly to a 40 mL capacity glass beaker. The ethanol was gradually added to the epoxy, then stirred with a magnetic stirrer at a speed of 500 rpm for 15 minutes to create a homogeneous solution. Once the epoxy resin and ethanol were well mixed together, 8 mL of hardener was accurately measured and added to the solution. The stirring was continued for another 10 minutes to enable proper absorption of the hardener into the epoxy/ethanol solution.

The pre-synthesized epoxy/ethanol solution was then coated onto the MgAZ61 alloy substrate, which had previously been polished using a spin coating machine. The substrate was positioned at the center of the spin coater's base. Four drops of epoxy solution was dropped onto the substrate, and the spin-coating process began at 1000 rpm for 30 seconds. Gradually, the speed decreased so that the coating was smoothly spread across the entire surface as a uniform layer. The spin coating process was performed at a constant speed of 1000 rpm, with four drops of coating solution applied to each substrate. Both the spinning speed and the volume of coating solution were kept constant across all samples to ensure uniform layer thickness among the coated substrates.

Subsequent to the spin coating, the coated substrate was cured at 60°C for two hours in order to harden the epoxy matrix and enhance its mechanical and chemical characteristics. Curing of the coating facilitated the adherence of the coating onto the substrate as well as provided a uniform foundation for additional testing and analysis.

3.3.4. Preparation of the X wt% ZnO/Epoxy Coating Solution and Application Process

Preparation of the 1.36 wt% ZnO/epoxy coating was properly carried out to achieve uniform dispersion of ZnO nanoparticles in the epoxy matrix and a good quality coating. The 1.36 wt% ZnO nanoparticles were subsequently transferred into a 10 mL capacity glass beaker with ethanol. The solution was mixed using a magnetic stirrer for 20 minutes to achieve initial dispersion of the nanoparticles. in order to achieve complete and uniform dispersion, the solution was subjected to ultrasonic treatment for 20 minutes in an ultrasonic processor, breaking the agglomerates and creating a homogenous suspension of ZnO and ethanol.

Afterward, 20 mL of epoxy resin was mixed with the ZnO/ethanol solution. The solution was transferred to a 40 mL glass beaker and stirred with a magnetic stirrer for 15 minutes to mix the epoxy resin well into the solution. After that, 8 mL of hardener was added to the solution and stirred for another 10 minutes to complete preparing the coating solution. The coating was deposited on the polished MgAZ61 alloy substrate

by a spin coating machine with a speed of 1000 rpm for 30 seconds and volume of 4 drops. Lastly, the coated substrate was cured at 60°C for two hours to cure the epoxy matrix and harden the coating. The above process was repeated to prepare solutions and coatings with different ZnO concentrations by varying weight percentages of ZnO nanoparticles while maintaining the amounts of epoxy resin, hardener, and ethanol constant. These different wt% solutions were 2.53 wt%, 4.10 wt%, and 5.20 wt%, to examine the effect of ZnO content on the coating's performance and characteristics.

3.3.5. Preparation of the GO/ZnO/Epoxy Coating Solutions

The preparation of the GO/ZnO/epoxy coating followed a systematic approach, similar to the steps used for ZnO/epoxy coatings, with additional care taken to ensure proper dispersion of graphene oxide (GO). At this stage, varying weight percentages of GO were incorporated into the ZnO/ethanol solution, while the quantities of ethanol, epoxy resin, and hardener were kept constant. The ZnO content was fixed at its optimum value, as determined from Tafel and EIS experiments for maximum corrosion resistance and was maintained across all GO-modified samples. GO concentrations of 0.8%, 0.4%, 0.2%, and 0.05% were investigated.

Following the addition of GO, the solution was stirred using a magnetic stirrer for 25 minutes to ensure the incorporation of GO particles into the dispersion. The ZnO/GO/ethanol solution was then subjected to ultrasonic treatment for an additional 25 minutes to enhance the uniformity of the suspension and prevent agglomeration of GO particles.

After dispersion, 20 mL of epoxy resin was added to the ZnO/GO/ethanol solution and transferred to a 40 mL glass beaker. The solution was stirred for 15 minutes using a magnetic stirrer to obtain a homogeneous solution of the resin with the dispersed GO and ZnO particles. Subsequently, 8 mL of hardener was added, and the solution was stirred for a further 10 minutes to complete the preparation process. The resulting solution was applied to the polished MgAZ61 alloy substrate using a spin coater with speed of 1000 rpm for 30 seconds and volume of 4 drops. The coated substrate was then cured at 60 °C for two hours to solidify the epoxy matrix.

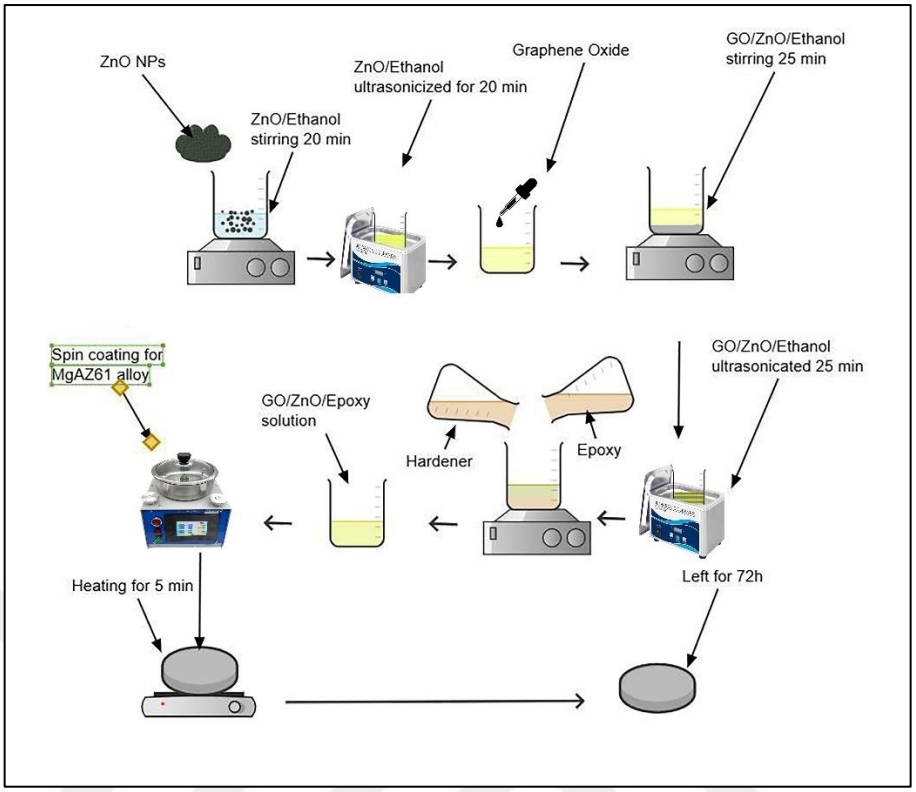

Figure 3.2. Sketch of preparation method for GO_x/ZnO_y/epoxy nanocomposite coating.

Figure 3.3. MgAZ61 substrate coated with GO/ZnO/Epoxy nanocomposite

3.4. ELECTROCHEMICAL CHARACTERIZATION

Electrochemical characterization of the prepared coatings was performed using a three-electrode electrochemical cell to evaluate their electrochemical behavior and potentiodynamic polarization performance. The primary techniques employed were Electrochemical Impedance Spectroscopy (EIS) and Tafel polarization tests, both of which provided valuable insight into the protective capabilities of the coatings applied to the MgAZ61 alloy substrate.

A Gamry electrochemical workstation Figure3.6 was used for all electrochemical measurements. It enables the assessment of both kinetic parameters and barrier properties in metallic and polymeric systems, making it particularly suitable for evaluating the corrosion resistance and performance of protective coatings.

Figure 3.4. Gamry potentiostat interface 1010.

3.4.1. Application for EIS and Tafel Tests

The Tafel and EIS tests are among the most informative tests regarding the nature of coatings and their electrochemical and mechanical properties. The coating resistance $\boldsymbol{R_c}$, charge transfer resistance $\boldsymbol{R_{ct}}$, solution resistance $\boldsymbol{R_s}$, constant phase element for the coating $\boldsymbol{CPE_c}$, and double-layer capacitance $\boldsymbol{CPE_{dl}}$ determined from the resultant impedance response provided essential insights into the barrier effectiveness of the coating against corrosion. Additionally, the Tafel polarization test measured the

corrosion potential (E_{corr}) and corrosion current density (I_{corr}), enabling the determination of the corrosion rate and protective efficiency of the coatings.

3.4.2. Components of Electrochemical Cell

The electrochemical cell was specially designed for accuracy and reproducibility Figure 3.7, and consisted of the following components:

1. **Working Electrode (WE)**: The coated MgAZ61 alloy substrate was used as the working electrode. It was encapsulated in Teflon to ensure that only the coated surface was exposed to the electrolyte, focusing the measurement accurately.
2. **Reference Electrode (RE)**: A saturated calomel electrode (SCE) provides a stable and constant reference potential.
3. **Counter Electrode (CE)**: A platinum electrode served as the counter electrode, completing the circuit and ensuring efficient current flow.
4. **Electrolyte Solution**: A 3.5% NaCl solution, prepared using analytical-grade NaCl supplied by ITK Chemicals and distilled water, was used to simulate a corrosive environment for the tests.

The cell was assembled in a clean and controlled environment to avoid contamination. The electrolyte was replaced after each specimen measurement to maintain uniform testing conditions.

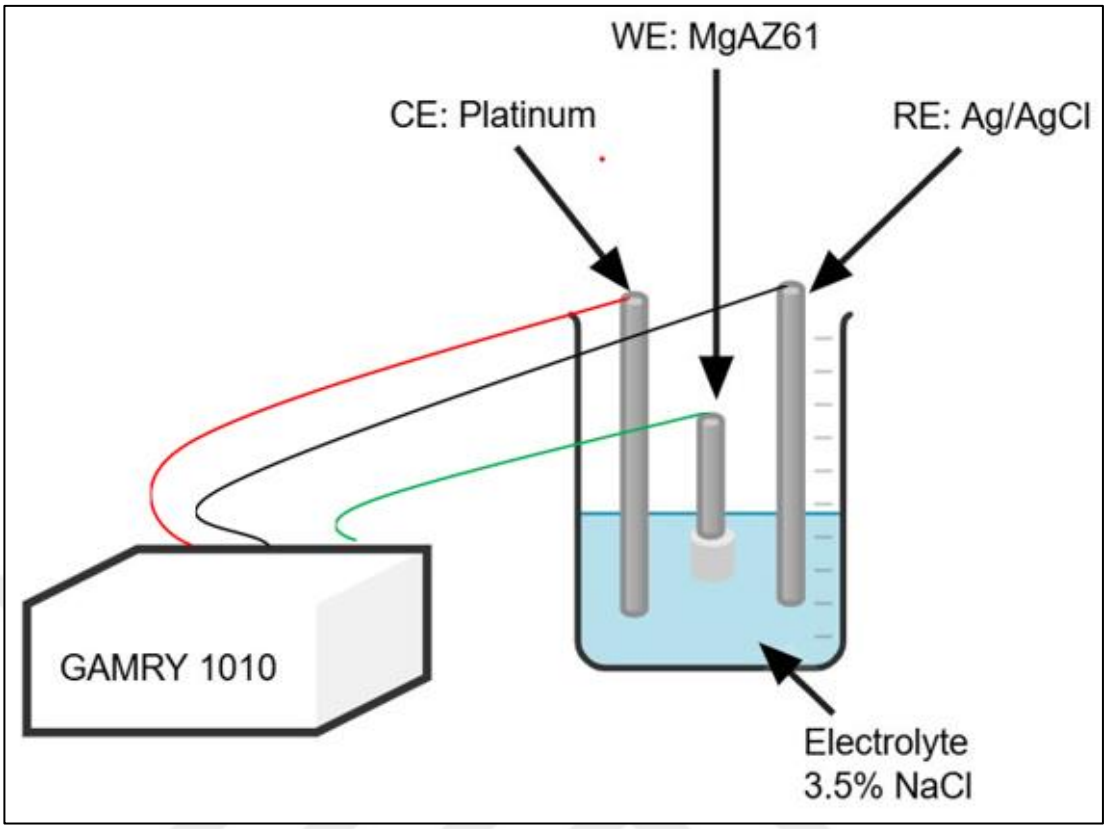

Figure 3.5. Three-electrodes electrochemical cell.

3.4.3. Data Analysis

3.4.3.1. EIS Data Analysis

1. **Nyquist Plots**: Nyquist plots represent the real impedance (Z′) versus the imaginary impedance (Z″). The diameter of the semicircle reflects the charge transfer resistance ($\boldsymbol{R_{ct}}$), a key parameter indicating the coating's resistance to ion transfer. A larger semicircle radius corresponds to greater corrosion resistance.
2. **Bode Plots**: Bode plots display the impedance magnitude (|Z|) and phase angle (θ) as functions of frequency. The |Z| value in the low-frequency region corresponds to the overall resistance of the coating, while the phase angle indicates the coating's capacitive behavior.

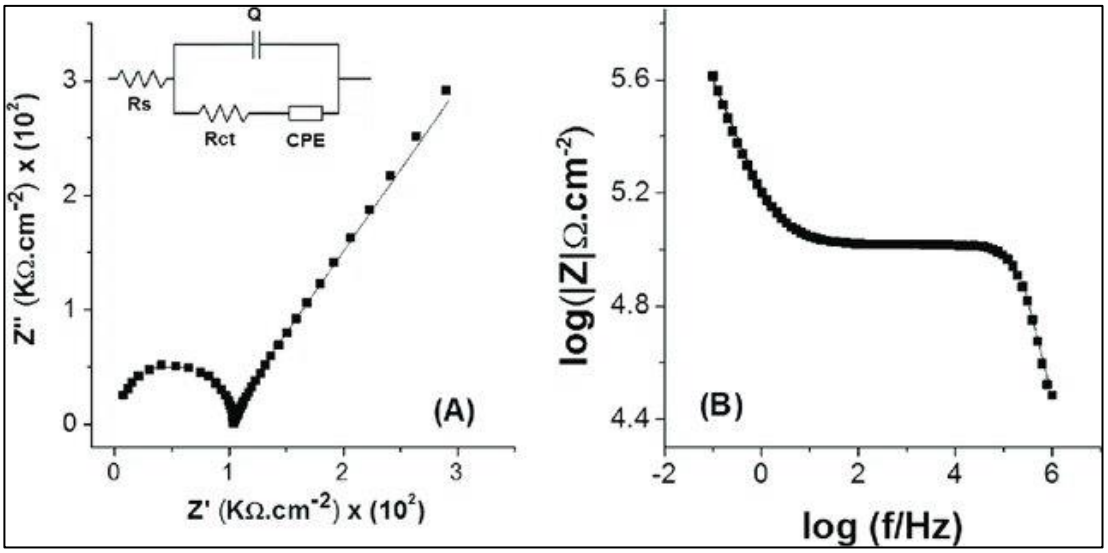

Figure 3.6. Sketch of Bode and Nyquist plots.

3.4.3.2. Tafel Polarization Analysis:

1. **Determination of E_{corr} and I_{corr}**: The corrosion potential (E_{corr}) and corrosion current density (I_{corr}) were extracted from the Tafel polarization curves. This was done by extrapolating the linear regions of the anodic and cathodic branches of the polarization curve to their intersection, representing the corrosion potential. The current at this intersection corresponds to the corrosion current density.

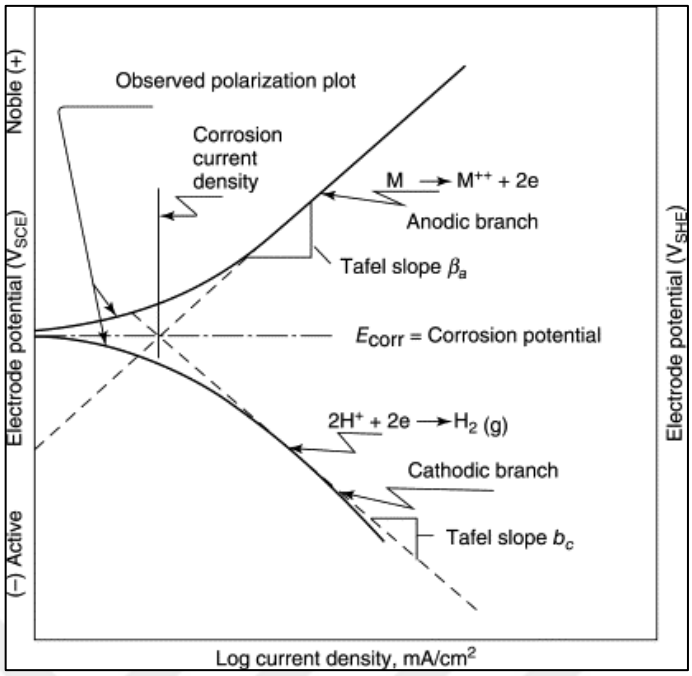

Figure 3.7. Sketch of the parameters obtained by Tafel plot.

2. **Corrosion Rate (CR) Calculation**: The equation for calculating corrosion rate from Tafel polarization data is grounded in Faraday's law and is standardized in ASTM G102-23. This standard provides a method to determine the corrosion rate (CR) using the current density (***I_{corr}***) equivalent weight (EW), and density (ρ) of the material. The formula is expressed as:

$$\mathrm{CR} = \frac{\mathrm{K} \cdot \mathrm{I_{corr}} \cdot \mathrm{EW}}{\rho} \tag{3.1}$$

Where K is a constant 3.27×10^3, $\mathrm{I_{corr}}$ is the corrosion current density (A/cm^2), EW is the equivalent weight of the material (g/equivalent), P is the density of the material (g/cm^3).

3.4.4. Key Information About the Tests

1. **Experimental Arrangement**: A copper rod was embedded in the MgAZ61 alloy, and the working electrode was connected and fixed with conductive adhesive.

2. **Instrumentation**: All tests were performed using a Gamry potentiostat controlled by its software, allowing for precise control of test parameters and real-time data acquisition.
3. **Conditions**: The experiments were conducted at room temperature. Before starting each experiment, the open-circuit potential (OCP) was monitored to ensure system stability.
4. **Surface Area of the Working Electrode**: As surface area of the working electrode increases, the current density decreases, assuming the total current remains constant. For the sample used in EIS and potentiodynamic polarization tests, the surface area was 3.50 cm^2
5. **Density of MgAZ61 Alloy:** The density of the MgAZ61 alloy was recorded as 1.74 g/cm^3 and was used in subsequent calculations to determine the corrosion rate.
6. **EIS Frequency Range**: The frequency range for all scans measured was from 10^5 Hz to 10^{-2} Hz.
7. **Scan Parameters for Tafel Test**:
    1. Initial Potential: -0.25 V a value slightly below the open circuit potential (OCP) was entered.
    2. Final Potential: 0.25 V a value slightly above the OCP was specified to include the anodic and cathodic branches of the polarization curve.

3.5. CHARACTERIZATION MEASUREMENTS

3.5.1. Scanning Electron Microscopy (SEM)

Scanning Electron Microscopy is a powerful technique for investigating materials' surface morphology and microstructural features. In this paper, SEM was performed on coated MgAZ61 alloy substrates to determine the coatings' quality, uniformity, and integrity.

SEM's operating principles involve using a focused beam of high-energy electrons impinging on the specimen surface. Interaction of the electron beam with the sample results in several signals, including secondary and backscattered electrons, that form

detailed images of topography and composition. With high-resolution capability that can visualize features on the nanometer scale, SEM becomes particularly effective in analyzing the dispersion of both ZnO and GO within an epoxy matrix, along with defects, cracks, or any inconsistency on the surface of the coating.

The SEM analysis was carried out in a vacuum for the best imaging conditions, and the samples were handled very carefully to avoid contamination. The results of SEM contributed considerably towards the identification of the microstructure of the coating and therefore acted as a guide for understanding its protection and mechanical properties.

Figure 3.8. Scanning electron microscopy device.

3.5.2. Fourier Transform Infrared Spectroscopy (FTIR)

For identifying the chemical structure of nanocomposite coatings, FTIR is widely used. It provides an infrared spectrum of absorption or emission that acts like a molecular fingerprint of the material. In nanocomposite coatings, FTIR is essential in confirming composite formation and providing evidence for chemical bonding between different phases. This can detect characteristic peaks corresponding to specific functional groups, giving evidence of the interactions between the matrix and fillers. Besides that, FTIR can be useful in investigating chemical composition, such as key functional group identification and the degree of chemical modification or curing of the material. FTIR thus stands out as one of the important techniques for understanding and optimizing the performance of nanocomposite coatings.

Figure 3.9. Fourier infrared transform spectroscopy device.

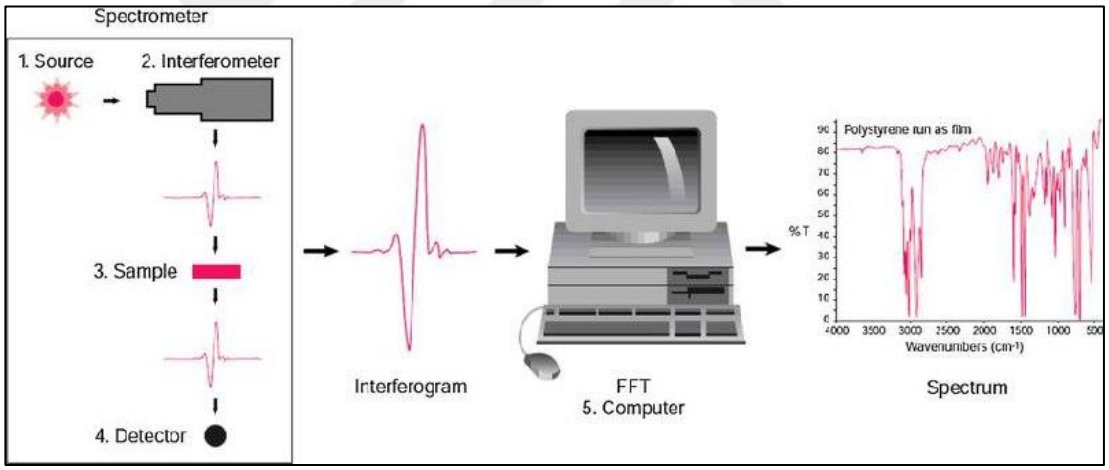

Figure 3.10. Working principle of FTIR testing.

3.5.3. Water Contact Angle (Wettability)

In nanocomposite coatings, the contact angle method (CAM) is widely used to assess surface properties. This technique gives information on the surface free energy of a material by analyzing the contact angle formed between a water droplet and the coating surface. The method effectively differentiates whether the surface is hydrophobic with a high contact angle greater than 90° or hydrophilic with a low contact angle less than 90°. This characterization is important in realizing the coating's protective and

functional properties, since wettability directly influences corrosion resistance, self-cleaning, and adhesion performance.

Figure 3.11. The device used to measure water contact angles.

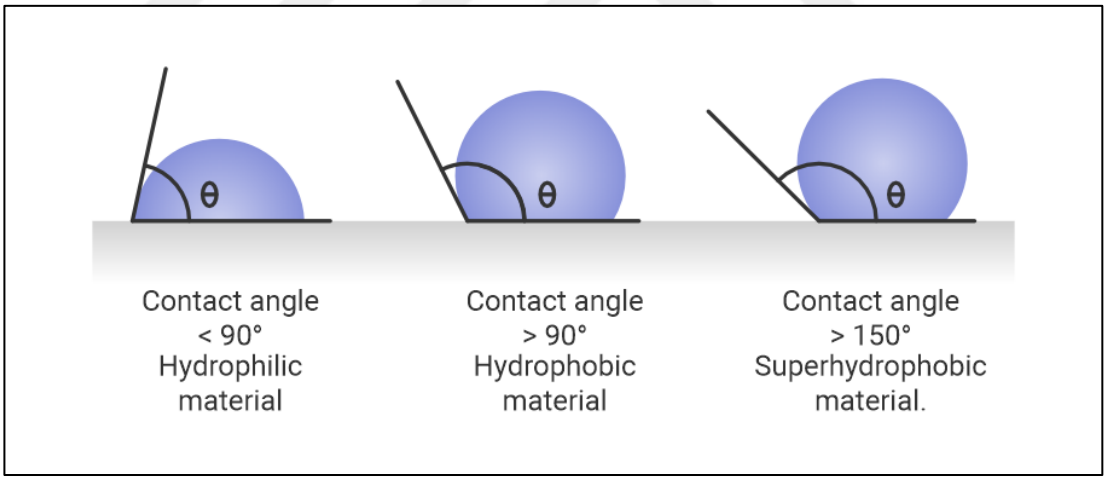

Figure 3.12. Hydrophobicity of materials according to water contact angle.

3.5.4. Thermogravimetric Analysis (TGA)

It includes analysis through thermogravimetry, characterized mainly by the measurement of mass variation, thermal stability, and composition of organic and inorganic materials, naturally occurring or synthetic, under conditions of programmed temperature variation, mostly under controlled atmosphere: inert or reactive. This

method can bring rich information on the behavior related to its decomposition, the temperature of maximum mass loss due to thermal degradation, and enable one to estimate the content of a volatile/stable component of the material.

In the context of nanocomposite coatings, TGA becomes an effective way to investigate the thermal stability of the coatings and their constituent parts. It allows for determining temperature intervals at which weight losses are most intensive, related to the destruction of organic phases, evaporation of volatile components, or decomposition of polymer matrices. This information is very important for the correct understanding of the resistance of the coating against thermal stress and its optimization for high-temperature applications.

TGA results mostly provide thermograms that plot weight loss against temperature, thus enabling the detection of distinct phases of decomposition and the quantification of relative stability for the different phases in the nanocomposite. In fact, this makes TGA a tool for assessing coating thermal properties and hence their reliability in practical applications.

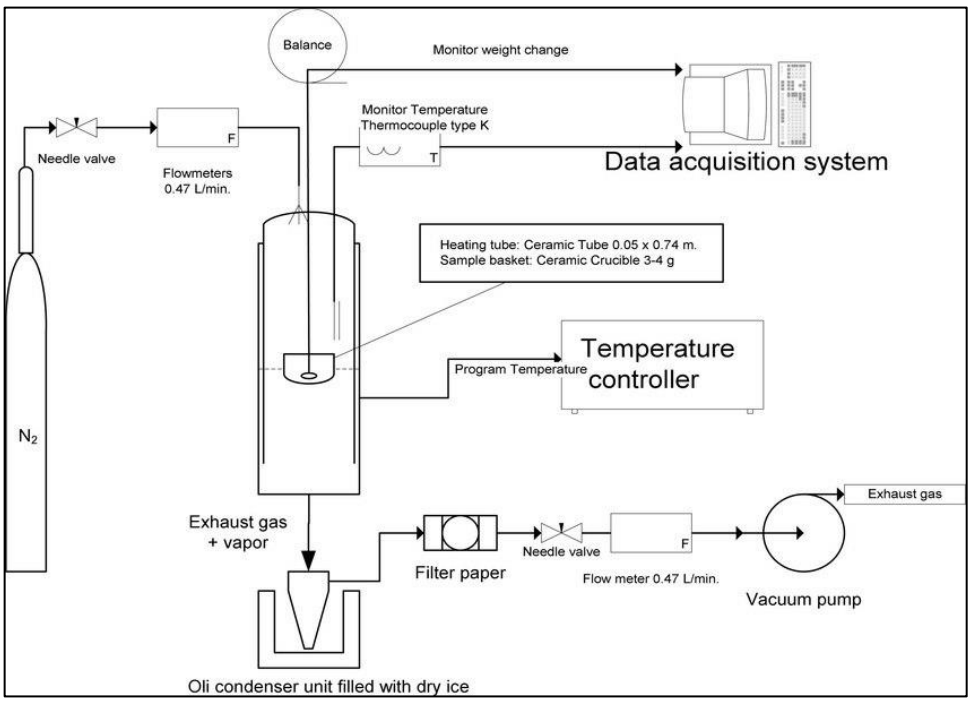

Figure 3.13. Working principle of thermogravimetric analyzer.

Figure 3.14. Automated system used in Thermogravimetric analysis.

3.5.5. Microhardness

Among the important properties that reflect resistance to micro-scale deformation of nanocomposite coatings under applied forces. The Vickers microhardness test is the most extensively used technique for determining this property in nanocomposite coatings. A diamond-shaped indenter is pressed into the coating surface under a specified load, and the size of the impression made is measured, yielding a quantitative measure of the hardness of the coating.

Figure 3.15. Microhardness measurements device.

3.5.6. X-ray Diffraction (XRD)

XRD is a powerful, non-destructive analytical technique that helps in the investigation of the crystalline structure of materials. It works on the principle of directing X-rays

onto a material and measuring diffraction patterns that are produced by the interaction of X-rays with the crystalline lattice. Such diffraction patterns give information about atomic arrangement, phase composition, crystallite size, and degree of crystallinity.

In the context of nanocomposite coatings, XRD is widely utilized for the identification and characterization of crystalline phases of nanomaterials embedded in the matrix, such as ZnO or GO. It can also detect changes in the crystalline structure because of interactions between the filler and the matrix.

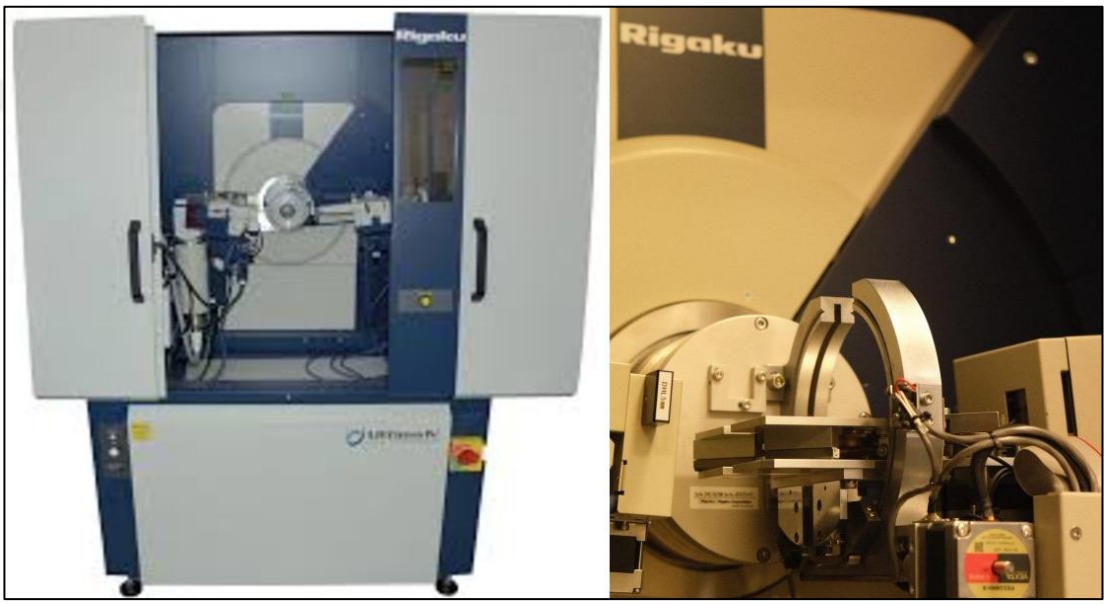

Figure 3.16. X-ray diffraction (XRD) instrument used for phase analysis.

CHAPTER 4

RESULTS and DISCUSSION

4.1. POTENTIODYNAMIC POLARIZATION (TAFEL) RESULTS

Tafel polarization curves of the bare substrate and epoxy-coated substrate, as shown in Figure 4.1 demonstrate significant differences in their Potentiodynamic Polarization properties. The epoxy-coated substrate exhibits a lower corrosion current density (I_{corr}) of 4.030×10^{-7}A/cm² as presented in Table 4.1, compared to the bare substrate, which has an I_{corr} of 6.682×10^{-7}A/cm². Additionally, the epoxy-coated substrate shows a higher corrosion potential (E_{corr}) of -1.333 V, in contrast to -1.523 V for the bare substrate. The corrosion rates of the bare substrate and the epoxy-coated substrate were determined to be 2940.9 mmpy and 854.4 mmpy, respectively. These results indicate that the lower I_{corr} and higher E_{corr} in the epoxy-coated substrate contributes to more effective anti-corrosion behavior of the coating [67].

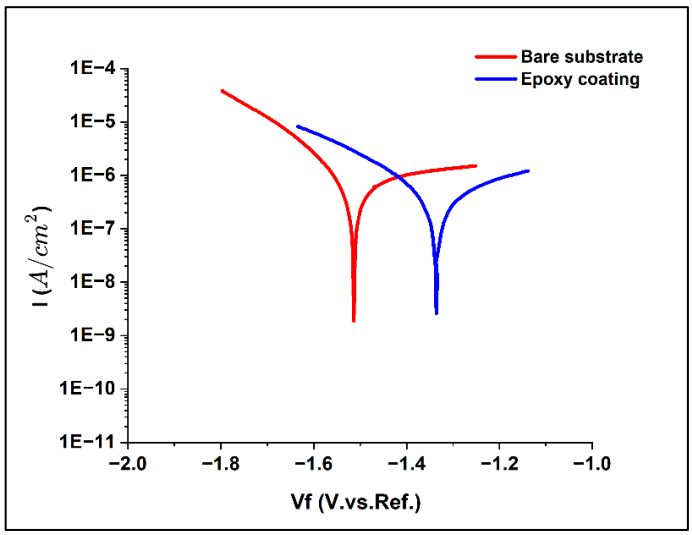

Figure 4.1. Tafel plots of bare substrate and epoxy-coated substrate.

Table 4.1. Tafel polarization results of bare substrate and epoxy coating.

Coating	I_{corr} (A/cm^2)	E_{corr} (V)	Corrosion Rate (mmpy)
Bare substrate	6.682×10^{-7}	-1.523	2940.9
Epoxy Coating	4.030×10^{-7}	-1.333	854.4

As mentioned earlier, the epoxy coating contains several micro-cracks, and to fill these cracks, ZnO nanoparticles were incorporated into the epoxy at different concentrations. These concentrations include $ZnO_{1.36}$/ep, $ZnO_{2.53}$/ep, $ZnO_{4.10}$/ep, and $ZnO_{5.20}$/ep. As observed in Figure 4.2 and Table 4.2, the increase in ZnO concentration directly influences both the I_{corr} and E_{corr} positively. According to the results, $ZnO_{4.10}$/ep exhibits the lowest I_{corr} and the highest E_{corr}, with values of 5.565×10^{-9} A/cm² and -0.518 V, respectively. In contrast, $ZnO_{1.36}$/ep exhibited the highest I_{corr} and the lowest E_{corr}, with va they have the opportunities of 3.486×10^{-7} A/cm² and -1.155 V, respectively. Despite this, its Potentiodynamic Polarization performance remains superior to that of the epoxy-coated substrate. The corrosion rates, as shown in Table 4.2, also reflect this trend. The corrosion rates for $ZnO_{1.36}$/ep, $ZnO_{2.53}$/ep, $ZnO_{4.10}$/ep, and $ZnO_{5.20}$/ep are 793.2 mmpy, 567.3 mmpy, 43.54 should be finemmpy, and 233.4 mmpy, respectively.

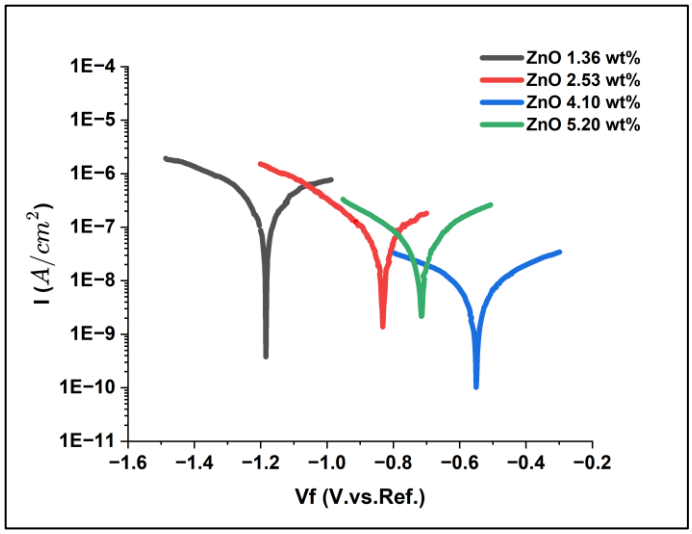

Figure 4.2. Tafel plots of $ZnO_{1.36}$/ep, $ZnO_{2.53}$/ep, $ZnO_{4.10}$/ep and $ZnO_{5.20}$/ep coatings.

Table 4.2. Tafel polarization results of $ZnO_{1.36}$/epoxy coating, $ZnO_{2.53}$/epoxy coating, $ZnO_{4.10}$/epoxy coating, and $ZnO_{5.20}$/epoxy coating.

Coating	I_{corr} *(A/cm²)*	E_{corr} (V)	*Corrosion Rate (mmpy)*
$ZnO_{1.36}$/epoxy	3.486×10^{-7}	-1.155	793.2
$ZnO_{2.53}$/epoxy	5.300×10^{-8}	-0.808	193.3
$ZnO_{4.10}$/epoxy	5.565×10^{-9}	-0.518	43.54
$ZnO_{5.20}$/epoxy	3.750×10^{-8}	-0.713	233.4

To further enhance the Potentiodynamic Polarization and mechanical properties of the coatings, four different concentrations of graphene oxide (GO) were dispersed with $ZnO_{4.10}$, which was selected as the optimal ZnO concentration. The GO/ZnO/ep coatings investigated include $GO_{0.8}/ZnO_{4.10}$/ep, $GO_{0.4}/ZnO_{4.10}$/ep, $GO_{0.2}/ZnO_{4.10}$/ep, and $GO_{0.05}/ZnO_{4.10}$/ep, as illustrated in Figure 4.3. It can be deduced that a decrease in GO concentration leads to a reduction in I_{corr} and an increase in E_{corr}. An increase in the graphene oxide (GO) content within the coating may lead to an elevated corrosion rate, primarily due to the propensity of GO nanoparticles to agglomerate when present in excessive amounts. While a limited concentration of GO enhances the barrier properties of the coating by creating tortuous diffusion pathways for corrosive species, an excessive presence can result in poor dispersion within the epoxy matrix. This agglomeration may contribute to the formation of micro-cracks and voids, thereby compromising the protective efficacy of the coating [41]. The results shown in Table 4.3. indicate that the $GO_{0.05}/ZnO_{4.10}$/ep coating exhibits the most favorable Potentiodynamic Polarization performance, with the lowest I_{corr} of 4.5 × 10^-9 A/cm² and the highest E_{corr} of -0.538 V. Conversely, the $GO_{0.8}/ZnO_{4.10}$/ep coating exhibits the highest I_{corr} of 2.500×10^{-7}A/cm² and lowest E_{corr} of -0.538 V. Moreover, the corrosion rates of $GO_{0.8}/ZnO_{4.10}$/ep, $GO_{0.4}/ZnO_{4.10}$/ep, $GO_{0.2}/ZnO_{4.10}$/ep, and $GO_{0.05}/ZnO_{4.10}$/ep coatings were determined to be 442.4 mmpy, 234.3 mmpy, 195.1 mmpy, and 4.170 mmpy, respectively.

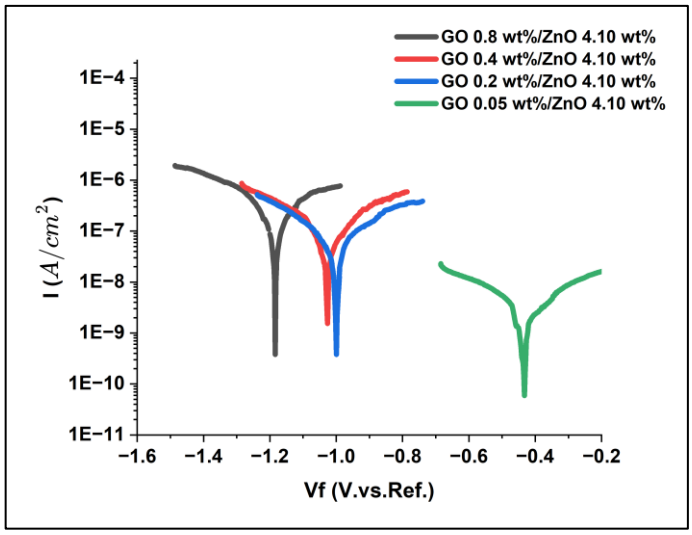

Figure 4.3. Tafel plots of $GO_{0,8}/ZnO_{4.10}$/ep. $GO_{0,4}/ZnO_{4.10}$/ep, $GO_{0,2}/ZnO_{4.10}$/ep and $GO_{0,05}/ZnO_{4.10}$/ep coatings.

Table 4.3. Tafel polarization results of $GO_{0.8}/ZnO_{4.1}$/epoxy, $GO_{0.4}/ZnO_{4.1}$/epoxy, $GO_{0.2}/ZnO_{4.1}$/epoxy and $GO_{0.05}/ZnO_{4.1}$/epoxy.

Coating	I_{corr} *(A/cm²)*	E_{corr} *(V)*	*Corrosion Rate (mmpy)*
$GO_{0.8}/ZnO_{4.1}$/epoxy	2.500×10^{-7}	-1.180	442.4
$GO_{0.4}/ZnO_{4.1}$/epoxy	1.900×10^{-7}	-1.024	234.3
$GO_{0.2}/ZnO_{4.1}$/epoxy	5.856×10^{-8}	-0.997	195.1
$GO_{0.05}/ZnO_{4.1}$/epoxy	3.485×10^{-9}	-0.422	4.170

With immersing the bare substrate, epoxy-coated substrate, $ZnO_{4.10}$/ep, and $GO_{0.05}/ZnO_{4.10}$/ep samples in a 3.5 wt% NaCl solution for 72 hours to evaluate the changes in Potentiodynamic Polarization performance, as illustrated in Figure 4.4 [a,b], a noticeable increase in the corrosion current density I_{corr} was observed for each sample, accompanied by a decrease in potential E_{corr}. The corrosion rates, as presented in Table 4.4 and Table 4.5, were determined to be 3212.4 mmpy, 1226.1 mmpy, 171.3 mmpy, and 113.7 mmpy for the bare substrate, epoxy-coated substrate, $ZnO_{4.10}$/ep, and $GO_{0.05}/ZnO_{4.10}$/ep, respectively.

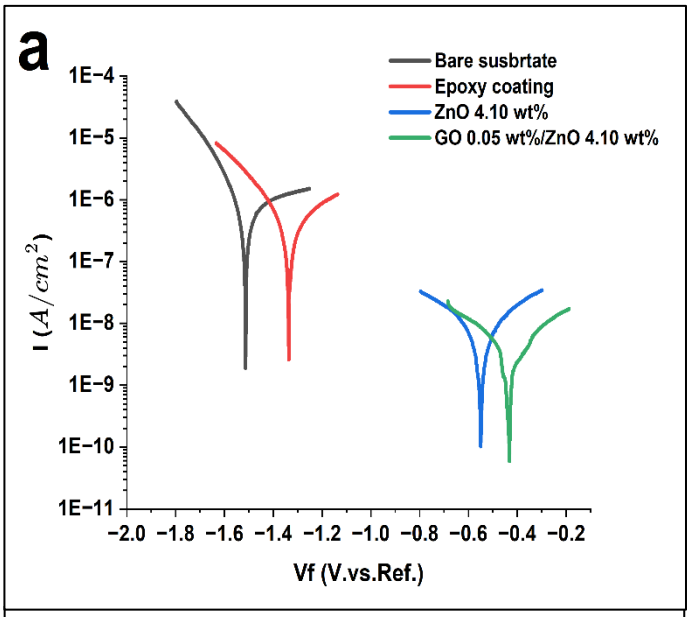

a) Tafel polarization plots are shown for bare substrate, epoxy-coated substrate, $ZnO_{4.10}$/ep, and $GO_{0.05}/ZnO_{4.10}$/ep samples before immersing in 3.5 wt% NaCl solution.

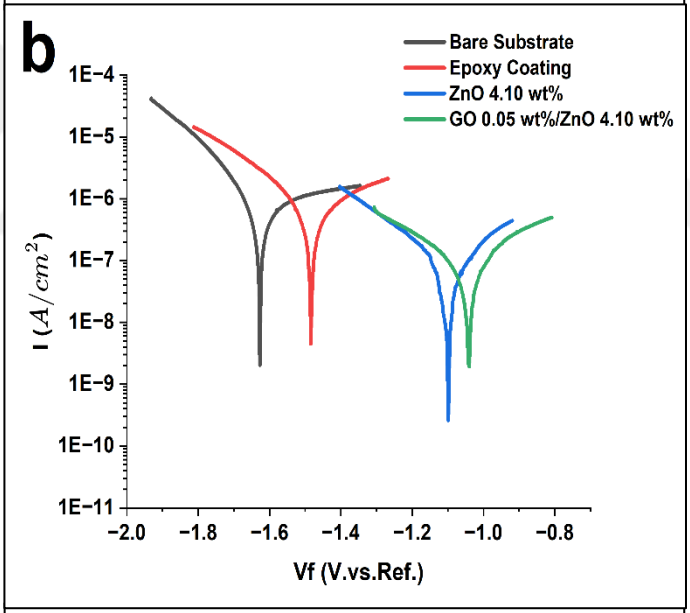

b) bare substrate, epoxy-coated substrate, $ZnO_{4.10}$/ep, and $GO_{0.05}/ZnO_{4.10}$/ep samples after immersing in 3.5 NaCl solution for 72h.

Figure 4.4. Tafel polarization plots are shown for : a) bare substrate, epoxy-coated substrate, $ZnO_{4.10}$/ep, and $GO_{0.05}/ZnO_{4.10}$/ep samples before immersing in 3.5 wt% NaCl solution, b) bare substrate, epoxy-coated substrate, $ZnO_{4.10}$/ep, and $GO_{0.05}/ZnO_{4.10}$/ep samples after immersing in 3.5 NaCl solution for 72h.

Table 4.4. Tafel polarization results of bare substrate, epoxy-coated substrate, $ZnO_{4.10}$/ep, and $GO_{0.05}/ZnO_{4.10}$/ep without immersing in 3.5% NaCl solution.

Coating	I_{corr} (A/cm^2)	E_{corr} (V)	Corrosion Rate (mmpy)
Bare substrate	6.682×10^{-7}	-1.523	2940.9
Epoxy coating	4.030×10^{-7}	-1.333	854.4
$ZnO_{4.10}$/ep	5.565×10^{-9}	-0.518	43.54
$GO_{0.05}/ZnO_{4.1}$/ep	3.485×10^{-9}	-0.422	4.170

Table 4.5. Tafel polarization results of bare substrate, epoxy-coated substrate, $ZnO_{4.10}$/ep, and $GO_{0.05}/ZnO_{4.10}$/ep with immersing in 3.5% NaCl solution.

Coating	I_{corr} (A/cm^2)	E_{corr} (V)	Corrosion Rate (mmpy)
Bare substrate	7.100×10^{-7}	-1.622	3212.4
Epoxy coating	5.800×10^{-7}	-1.406	1226.1
$ZnO_{4.10}$/ep	7.920×10^{-8}	-1.040	171.3
$GO_{0.05}/ZnO_{4.1}$/ep	4.660×10^{-8}	-1.047	113.7

4.2. ELECTROCHEMICAL IMPEDANCE SPECTROSCOPY (EIS) RESULTS

Electrochemical Impedance Spectroscopy (EIS) is a well-established technique for evaluating the anti-corrosion performance of epoxy-based coatings. The impedance spectra of the bare MgAZ61 substrate, epoxy-coated substrate, ZnO_x/ep coatings, and GO_x/ZnO_x/ep composite coatings were systematically analyzed. The Nyquist plots of the bare substrate and epoxy-coated substrate Figure 4.5 clearly demonstrate that the epoxy-coated sample exhibits a significantly higher impedance value (54,232 Ω·cm²) compared to the bare substrate (28,150 Ω·cm²) as illustrated in Table 4.6.

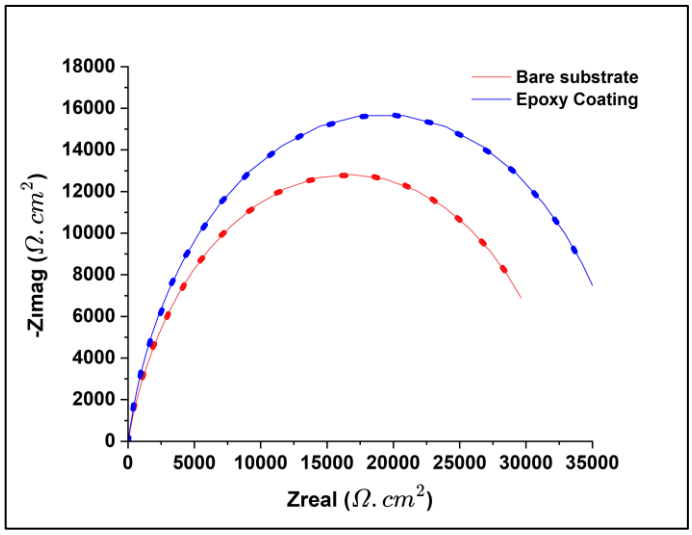

Figure 4.5. Nyquist plots of bare substrate and epoxy-coated substrate.

Table 4.6. EIS fitted Nyquist curve's results of bare substrate. epoxy coating.

Coating	R_{ct} (Ωcm^{-2})	R_s (Ωcm^{-2})	R_c (Ωcm^{-2})	CPE_{dl} ($\Omega^{-1} cm^{-2} s^n$)	CPE_c ($\Omega^{-1} cm^{-2} s^n$)
Bare Substrate	28150	25.46	-	94.02×10^{-6}	-
Epoxy Coating	54232	22.83	38020	$7.318\times\mathbf{10^{-6}}$	$11.37\times\mathbf{10^{-6}}$

The incorporation of ZnO nanoparticles at varying weight percentages into the epoxy matrix resulted in a substantial enhancement of the coating's impedance, as depicted in Figure 4.6. A comparative analysis of the Nyquist plots for $ZnO_{1.36}$/ep coating. $ZnO_{2.53}$/ep, $ZnO_{4.10}$/ep, $ZnO_{5.20}$/ep coatings reveal a notable improvement in impedance values. Among these formulations, the $ZnO_{4.10}$/ep coating exhibited the highest impedance value of 129,000 Ω·cm² as observed in Table 4.6, surpassing $ZnO_{1.36}$/ep (57,105 Ω·cm²), $ZnO_{2.53}$/ep (81,440 Ω·cm²), and $ZnO_{5.20}$/ep (113,580 Ω·cm²).

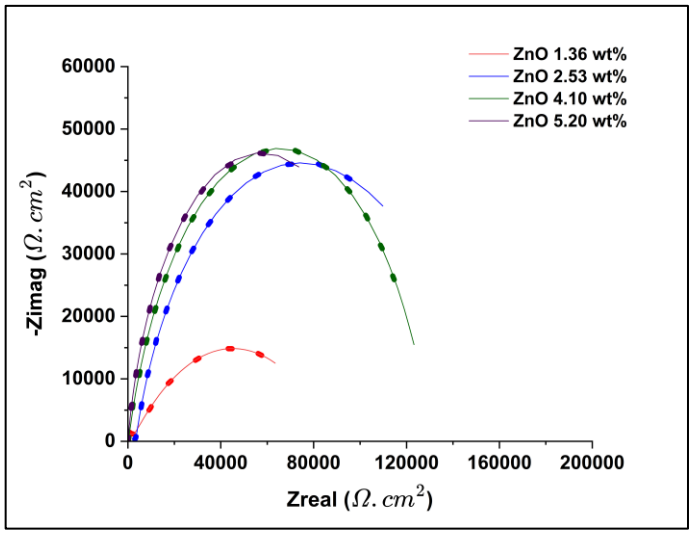

Figure 4.6. Nyquist plots of $ZnO_{1.36}$/ep, $ZnO_{2.53}$/ep, $ZnO_{4.10}$/ep and $ZnO_{5.20}$/ep coatings.

Table 4.7. EIS fitted Nyquist curve's results of $ZnO_{1.36}$/epoxy coating, $ZnO_{2.53}$/epoxy coating, $ZnO_{4.10}$/epoxy coating, and $ZnO_{5.20}$/epoxy coating.

Coating	R_{ct} (Ωcm^{-2})	R_s (Ωcm^{-2})	R_c (Ωcm^{-2})	CPE_{dl} ($\Omega^{-1}cm^{-2}s^n$)	CPE_c ($\Omega^{-1}cm^{-2}s^n$)
$ZnO_{1.36}$/ep	57105	11.72	33030	6.276×10^{-6}	8.627×10^{-6}
$ZnO_{2.53}$/ep	81440	33.71	1681	5.394×10^{-6}	7.326×10^{-6}
$ZnO_{4.10}$/ep	129000	0.232	3705	4.248×10^{-6}	9.024×10^{-7}
$ZnO_{5.20}$/ep	113580	$20.1\times\mathbf{10^{-6}}$	264.7	$4.376\times\mathbf{10^{-6}}$	$2.160\times\mathbf{10^{-6}}$

To further augment both the electrochemical and mechanical properties of the $ZnO_{4.10}$/ep coating, graphene oxide (GO) nanoparticles were introduced at different weight percentages. The Nyquist plots of $GO_{0.8}/ZnO_{4.1}$/ep, $GO_{0.4}/ZnO_{4.1}$/ep, $GO_{0.2}/ZnO_{4.1}$/ep and $GO_{0.05}/ZnO_{4.1}$/ep coatings, presented in Figure 4.7, demonstrate a substantial enhancement in impedance with decreasing GO content. Notably, the $GO_{0.05}/ZnO_{4.1}$/ep coating exhibited the highest impedance value of 499,020 Ω·cm² according to the data in Table 4.8, significantly surpassing the values observed for $GO_{0.8}/ZnO_{4.1}$/ep (133,475 Ω·cm²), $GO_{0.4}/ZnO_{4.1}$/ep (165,420 Ω·cm²), and $GO_{0.2}/ZnO_{4.1}$/ep (319,050 Ω·cm²). These findings suggest that when ZnO (4.10 wt%) and GO (0.05 wt%) were incorporated as nanofillers into the epoxy coating, the

micropores within the coating matrix were effectively filled, thereby impeding the diffusion pathways of corrosive agents and significantly enhancing the corrosion resistance of the epoxy-based coating.

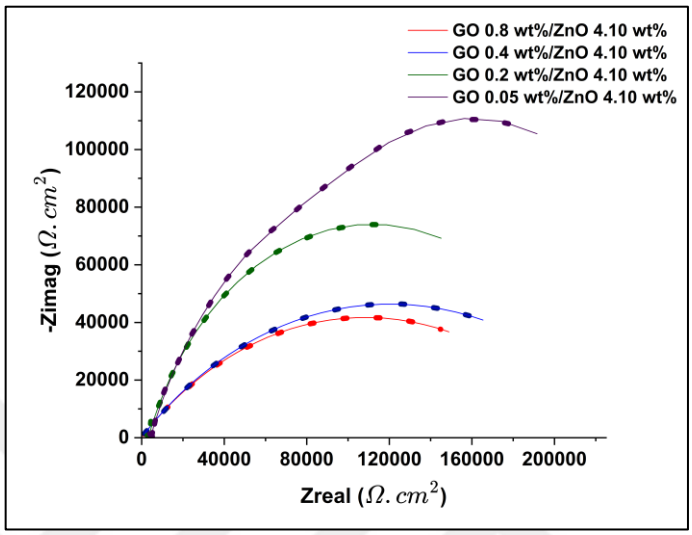

Figure 4.7. Nyquist plots of $GO_{0,8}/ZnO_{4.10}$/ep. $GO_{0,4}/ZnO_{4.10}$/ep, $GO_{0,2}/ZnO_{4.10}$/ep and $GO_{0,05}/ZnO_{4.10}$/ep coatings.

Table 4.8. EIS fitted Nyquist curve's results of$GO_{0.8}/ZnO_{4.1}$/epoxy. $GO_{0.4}/ZnO_{4.1}$/epoxy. $GO_{0.2}/ZnO_{4.1}/epoxy$ and $GO_{0.05}/ZnO_{4.1}$/epoxy.

Coating	R_{ct} (Ωcm^{-2})	R_s (Ωcm^{-2})	R_c (Ωcm^{-2})	CPE_{dl} ($\Omega^{-1}cm^{-2}s^n$)	CPE_c ($\Omega^{-1}cm^{-2}s^n$)
$GO_{0.8}/ZnO_{4.1}$/ ep	133475	6.607	3247	2.995×10^{-6}	6.913×10^{-8}
$GO_{0.4}/ZnO_{4.1}$/ ep	165420	7930	20210	1.758×10^{-6}	5.754×10^{-9}
$GO_{0.2}/ZnO_{4.1}$/ ep	319050	0.002	0.032	1.471×10^{-6}	7.869×10^{-10}
$GO_{0.05}/ZnO_{4.1}$ /ep	499020	657.4	84020	$7.864\times\mathbf{10^{-7}}$	$9.815\times\mathbf{10^{-11}}$

To quantitatively analyze the EIS data, equivalent circuit modeling was performed using Gamry software. The equivalent circuit, depicted in Figure 4.8, successfully fitted the experimental data, It is particularly noteworthy that the progressive reduction in CPE_{dl} and the concurrent increase in R_{ct} confirm that the $GO_{0.05}/ZnO_{4.1}$/ep coating exhibits the most favorable electrochemical properties [68,69], indicating that this

optimized formulation is the most structurally dense and effectively prevents the penetration of corrosive media into the underlying substrate [70,71].

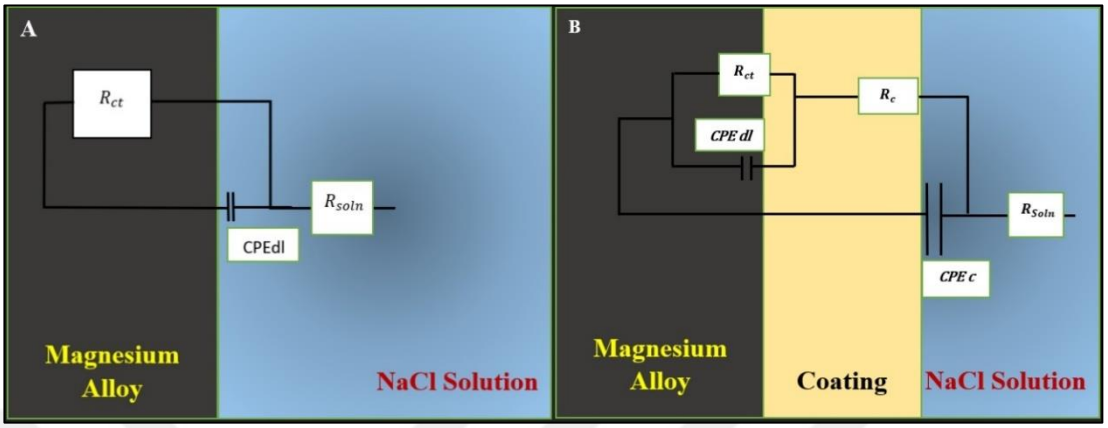

Figure 4.8. Equivalent circuits used to fit the EIS data of the bare MgAZ61 alloys A) and the coated MgAZ61 alloy B).

The Bode modulus of the bare MgAZ61 substrate, epoxy-coated substrate, ZnO_x/ep coatings, and GO_x/ZnO_x/ep was analyzed, where the impedance modulus at 0.01 Hz ($|Z|_{0.01Hz}$) is considered a critical electrochemical parameter for assessing the anti-corrosion performance of protective coatings. A higher Bode modulus is indicative of superior corrosion resistance [72]. The low-frequency impedance (Log |Z| at f = 0.01 Hz) for the epoxy-coated sample did not exceed 55,000 Ω·cm², which is significantly higher than that of the bare substrate, as shown in Figure 4.9, demonstrating the improved barrier performance conferred by the epoxy layer.

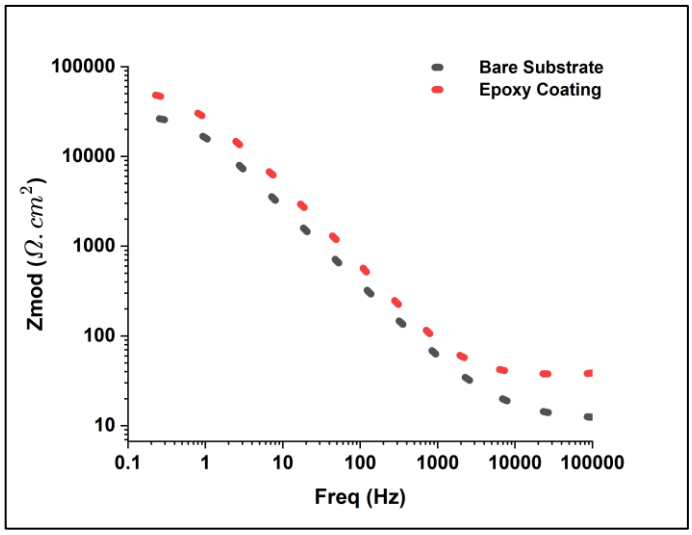

Figure 4.9. Bode plots of bare substrate and epoxy-coated substrate.

Furthermore, all epoxy-based coatings containing ZnO nanoparticles exhibited Log |Z| values exceeding 55,000 Ω·cm², as shown in Figure 4.10. Among the ZnO-modified coatings, $ZnO_{4.1}$/ep demonstrated the highest Bode modulus, with a Log |Z| value of 129,000 Ω·cm², highlighting its superior electrochemical performance compared to other ZnO formulations.

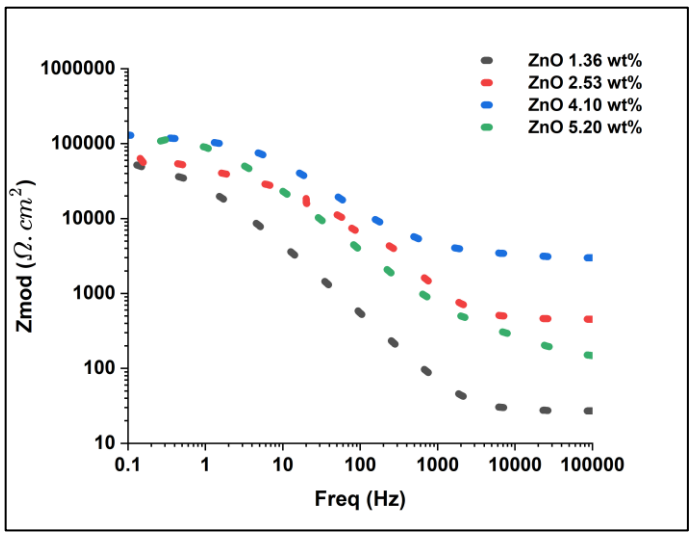

Figure 4.10. Bode plots of $ZnO_{1.36}$/ep, $ZnO_{2.53}$/ep, $ZnO_{4.10}$/ep and $ZnO_{5.20}$/ep coatings.

To further improve the protective properties of the $ZnO_{4.10}$/ep coating, graphene oxide (GO) was incorporated at varying weight percentages. The Bode modulus values for

$GO_{0.8}/ZnO_{4.1}$/ep, $GO_{0.4}/ZnO_{4.1}$/ep, $GO_{0.2}/ZnO_{4.1}$/ep, and $GO_{0.05}/ZnO_{4.1}$/ep are depicted in Figure 4.11, all of which exhibit impedance values exceeding 129,000 Ω·cm², confirming the enhanced corrosion resistance of GO-ZnO hybrid coatings. Notably, the $GO_{0.05}/ZnO_{4.1}$/ep coating exhibited the highest impedance value, reaching approximately 5×10^5 Ω·cm², marking a substantial improvement in barrier properties compared to other formulations.

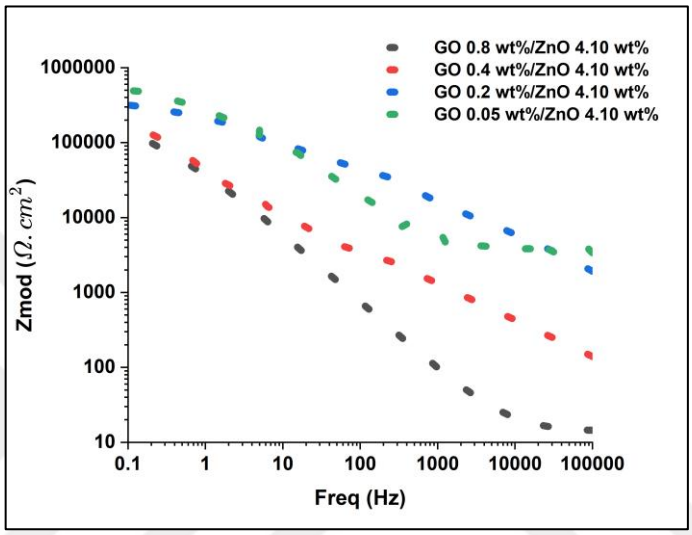

Figure 4.11. Bode plots of $GO_{0,8}/ZnO_{4.10}$/ep. $GO_{0,4}/ZnO_{4.10}$/ep, $GO_{0,2}/ZnO_{4.10}$/ep and $GO_{0,05}/ZnO_{4.10}$/ep coatings.

To further investigate the corrosion resistance of the developed coatings, electrochemical impedance spectroscopy (EIS) was employed to evaluate the performance of the bare MgAZ61 substrate, epoxy-coated substrate, $ZnO_{4.1}$/ep, and $GO_{0.05}/ZnO_{4.1}$/ep coatings with and without immersion in a 3.5 wt% NaCl solution for 72 hours. The Nyquist plots, as presented in Figure 4.12a, provide a comparative analysis of the electrochemical behavior of these coatings prior to immersion. Subsequently, after 72 hours of exposure to the simulated seawater environment, notable reductions in impedance values were observed, as illustrated in Figure4.12b, indicating a progressive decline in the corrosion resistance of all examined coatings. Despite this degradation, the $ZnO_{4.1}$/ep and $GO_{0.05}/ZnO_{4.1}$/ep coatings retained higher impedance values than both the epoxy-coated and bare substrates, highlighting their enhanced protective capabilities against electrolyte penetration and subsequent corrosion initiation. A quantitative analysis of the EIS parameters with and without

immersion, summarized in Table 4.10, further corroborates these observations. The results demonstrate a decrease in charge transfer resistance (R_{ct}) and an increase in the constant phase element of the double layer (CPE_{dl}) for all coatings following immersion, which is indicative of progressive coating degradation. Specifically, the bare MgAZ61 substrate exhibited an R_{ct} of 18,755 Ω·cm² and a CPE_{dl} of 1.254 × 10^{-4} Ω^{-1} cm^{-2} s^n, whereas the epoxy-coated substrate still displays improved corrosion resistance with a R_{ct} of 48,460 Ω·cm² and a CPE_{dl} of 9.651 × 10^{-6} Ω^{-1} cm^{-2} s^n. $ZnO_{4.1}$/ep coating, which exhibited an R_{ct} of 103,880 Ω·cm² and a CPE_{dl} of 7.321 × 10^{-6} Ω^{-1} cm^{-2} s^n which reveals better performance than bare and epoxy-coated substrats. Most notably, the $GO_{0.05}$/$ZnO_{4.1}$/ep coating demonstrated superior corrosion resistance, with the highest R_{ct} of 455,120 Ω·cm² and the lowest CPE_{dl} of 9.786 × 10^{-7} Ω^{-1} cm^{-2} s^n. Further insight into the degradation behavior of these coatings is provided by the Bode modulus analysis. As depicted in Figure 4.13a, prior to immersion, the Log |Z| at f = 0.01 Hz was significantly higher for the $GO_{0.05}$/$ZnO_{4.1}$/ep coating, followed by the $ZnO_{4.1}$/ep, epoxy-coated substrate, and bare substrate, reinforcing the superior initial barrier properties of the GO-ZnO hybrid coatings. However, following 72 hours of immersion, the Bode modulus values, as shown in Figure 4.13b, revealed a distinct reduction in Log |Z| at f = 0.01 Hz for all coatings, further confirming the deleterious effects of prolonged exposure to the NaCl solution. Despite this decline, the $GO_{0.05}$/$ZnO_{4.1}$/ep coating retained the highest impedance values, affirming its superior corrosion resistance even under extended immersion conditions. These findings unequivocally demonstrate that while all coatings experienced a reduction in electrochemical performance after exposure to a simulated seawater environment, the incorporation of ZnO and GO nanoparticles significantly enhanced the long-term stability and corrosion resistance of the epoxy coatings. The superior performance of $GO_{0.05}$/$ZnO_{4.1}$/ep is attributed to its ability to reduce microporosity, hinder the diffusion of corrosive species, and reinforce the physical integrity of the coating, thereby extending its protective efficacy.

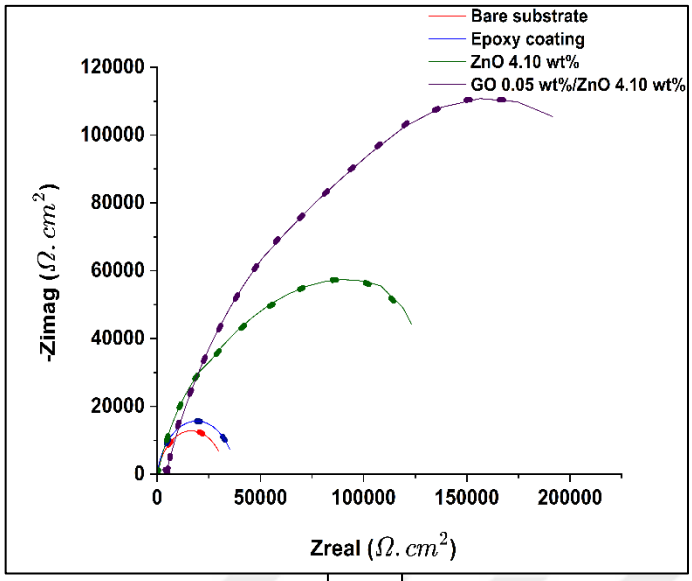

a.)

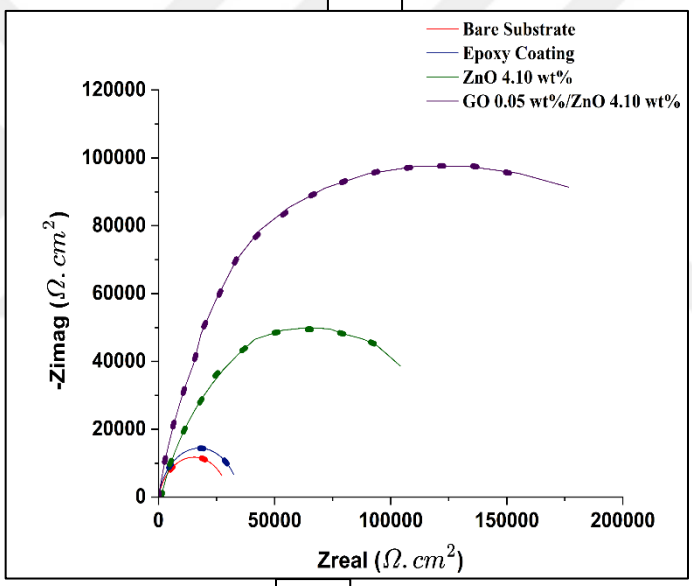

b.
)

Figure 4.12. The Nyquist plots of bare substrate, epoxy-coated substrate, $ZnO_{4.1}$/ep coating and $GO_{0.05}/ZnO_{4.1}$/ep coating .b) The Nyquist plots of bare substrate, epoxy-coated substrate, $ZnO_{4.1}$/ep coating and $GO_{0.05}/ZnO_{4.1}$/ep coating with 72h immersion in NaCl solution .

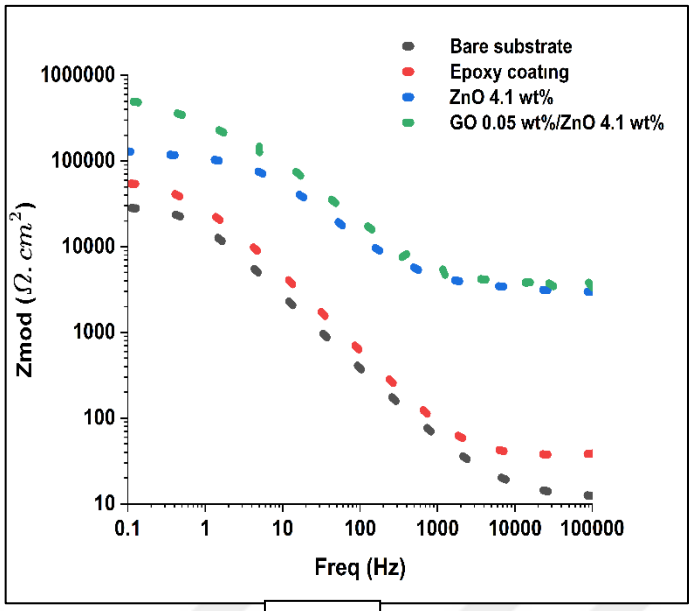

a.)

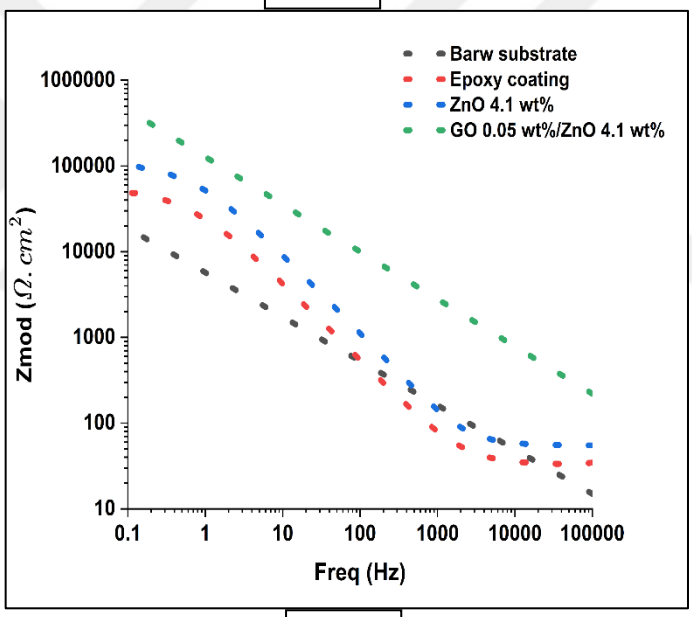

b.)

Figure 4.13. Bode plots of bare substrate, epoxy-coated substrate, $ZnO_{4.1}$/ep coating and $GO_{0.05}/ZnO_{4.1}$/ep coating a).The Bode plots of bare substrate, epoxy-coated substrate, $ZnO_{4.1}$/ep coating and $GO_{0.05}/ZnO_{4.1}$/ep coating with 72h immersion in NaCl solution b).

Table 4.9. EIS fitted Nyquist curve's results of bare substrate. epoxy coating. $ZnO_{4.10}$/epoxy and $GO_{0.05}/ZnO_{4.1}$/epoxy with and without immersion in NaCl for 72h.

Coating	R_{ct} (Ωcm^{-2})	R_s (Ωcm^{-2})	R_c (Ωcm^{-2})	CPE_{dl} $(\Omega^{-1}cm^{-2}s^n)$	CPE_c $(\Omega^{-1}cm^{-2}s^n)$
Bare substrate	28150	25.46	-	94.02×10^{-6}	-
Bare substrate in NaCl	18755	23.10	-	1.254×10^{-4}	-
Epoxy Coating	54232	22.83	38020	7.318×10^{-6}	11.37×10^{-6}
Epoxy Coating in NaCl	48460	22.16	35462	9.651×10^{-6}	12.41×10^{-6}
$ZnO_{4.1}$/epoxy	129000	0.232	3705	4.248×10^{-6}	9.024×10^{-7}
$ZnO_{4.1}$/epoxy in NaCl	103880	6.250×10^{-6}	2751	7.321×10^{-6}	2.054×10^{-6}
$GO_{0.05}/ZnO_{4.1}$/ep	499020	657.4	84020	7.864×10^{-7}	9.815×10^{-11}
$GO_{0.05}/ZnO_{4.1}$/ep in NaCl	455120	549.3	75021	9.786×10^{-7}	3.498×10^{-10}

The incorporation of ZnO-GO nanoparticles into epoxy-based coating systems enhances surface hydrophobicity by reducing hydrogen bonding and improving nanoparticle dispersion, thereby minimizing water penetration, as illustrated in Figure 4.14. Electrochemical Impedance Spectroscopy (EIS) was employed to evaluate the corrosion resistance of epoxy-coated MgAZ61 alloy, with and without ZnO nanoparticles, in a 3.5% NaCl solution. The ZnO/epoxy-coated samples exhibited improved resistance during wet–dry cycles, as indicated by higher charge transfer resistance (R_{ct}) and lower double-layer capacitance (CPE_{dl}) in the Nyquist plots. The formation of ZnO-containing corrosion products on scratched areas further contributed to the enhanced protection performance. [71].

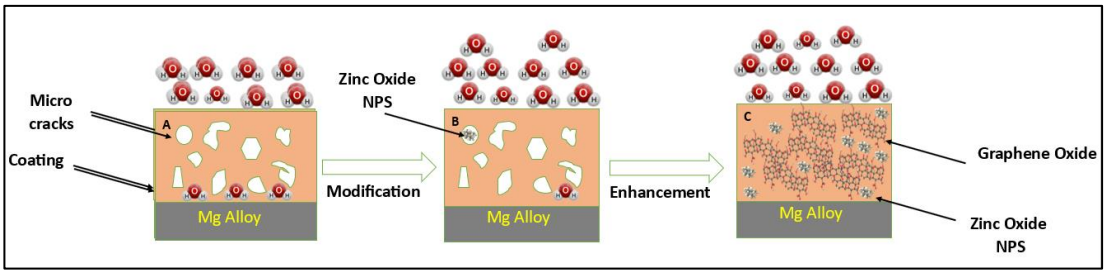

Figure 4.14. Schematic illustration on the enhanced anticorrosive mechanism. a), b), c) are epoxy-coated substrate, ZnO/ep modified coating and GO/ZnO/ep enhanced coating.

4.3. MORPHOLOGICAL CHARACTERIZATION

The epoxy-coated substrate possesses smooth and uniform morphology with microporous distribution on its surface, as shown in Figure 4.15a. The ordered dispersion of ZnO nanoparticles within the epoxy resin matrix was approved by FE-SEM image as illustrated in Figure 4.15b, which could be considered as evidence for the competence of the sonication process for increasing an applicable level of ZnO nanoparticles dispersion within the used epoxy resin matrix. However, it is notable that with the increasing mass density of nanoparticles, the ability of the particles to be attracted to each other increased, thus forming relatively heavier agglomerated particles in the epoxy resin matrix. Besides, the diverse morphology that could be shown on the epoxy resin matrix incorporation with the ZnO nanoparticles led to an extremely rough epoxy matrix, which guarantees a more hydrophobic epoxy matrix as shown in Figure 4.15c. In addition, it was also noticed that the best curing of ZnO/epoxy nanocomposite coatings is vital for preparing coatings without any micro-cracks, which reveals the robust interface between the epoxy binder and ZnO nanoparticles that endorses the greater barrier performance of the developed coatings. Moreover, some graphene oxide fillers cluster with ZnO nanoparticles on the developed coatings, denoting that the graphene oxide sheets reassemble to create bigger nanoparticles during the mixture with nanoparticles and epoxy resin. More notably, the internal microcracks and micropores were filled by graphene oxide on these developed coatings, which arguably are excellent protection barriers to prevent the permeable diffusion of corrosive ions. Furthermore, the elemental compositions regarding the proper GO and ZnO nanoparticles within the epoxy resin matrix were

obtained via the EDX spectra as shown in Fig. 4.15d, the presence of C, O, and Zn elements within the coating indicates that the hybrid of GO and ZnO nanoparticles have been successfully introduced to the epoxy resin matrix.

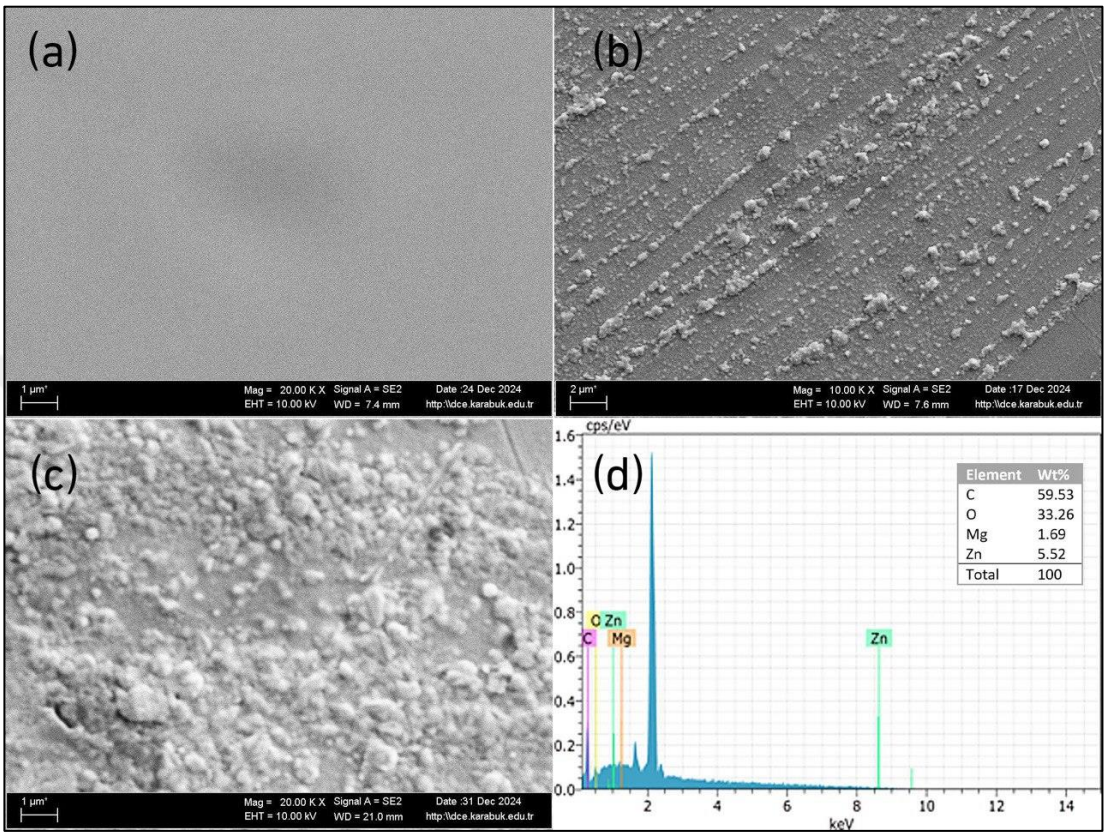

Figure 4.15. FE-SEM illustration of epoxy-coated substrate a), ZnO/ep coated substrate b), GO/ZnO/ep coated substrate c), and EDX spectra and elemental composition d).

4.4. STRUCTURAL AND CHEMICAL CHARACTERIZATION

4.4.1. X-ray Diffraction (XRD)

The x-ray diffraction patterns of the GO, GO/Ep, and GO/ZnO/Ep nanocomposites are typically shown in Figure 4.16 [a, b, and c], respectively. In the GO pattern, the sharp peak at 2θ value 11° appears due to the GO with inter-planar spacing (002) of GO as shown in Figure 4.16a. However, the epoxy exhibits broad peaks at 2θ values 21° and 48° due to the scattering from the epoxy's cross-linked network, indicating the amorphous nature of epoxy [73]. Serious studies of the XRD patterns for the epoxy

and its nanocomposite are found to be almost analogous [74]. Nevertheless, GO-Ep and GO/ZnO/Ep nanocomposites show all characteristic peaks of GO and ZnO that may occur due to the homogenous and cluster-free dispersion nanofiller in the entire epoxy matrix. At this time, the GO/Ep spectrum of the reflection peak (002) for pure GO at 2θ value equal 11° is shifted towards the 2θ value of 20.5° due to the intercalation of epoxy chains in the packed GO layers as shown in Figure 4.16b. Besides, the shifting of GO peak in the composites indicates the lamination of GO layers in the presence of epoxy. Moreover, the x-ray diffraction pattern of ZnO nanoparticles in the GO/ZnO/Ep spectrum shows sequences of peaks with 2θ values 32.08°, 34.41°, 36.35°, 56.72°, 62.95°, and 68° which are assigned to (100), (002), (101), (110), (103) and (112) planes of ZnO crystalline [75] , as shown in Figure 4.16c. The x-ray diffraction profiles also denote evidence of GO and ZnO nanofillers' full and homogeneous dispersion inside the epoxy matrix.

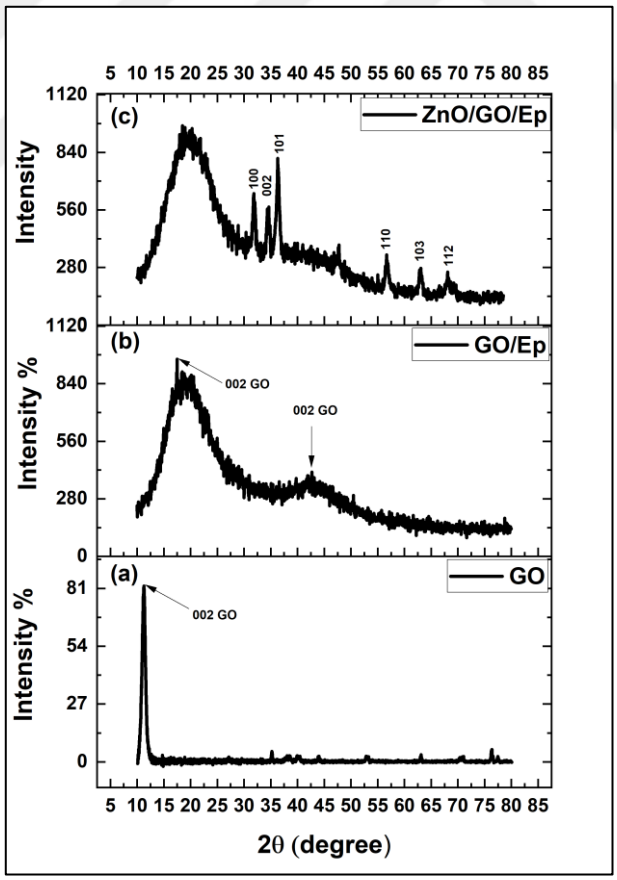

Figure 4.16. X-ray diffraction (XRD) patterns of a) graphene oxide (GO), b) GO/epoxy nanocomposite coating, and c) ZnO/GO/epoxy nanocomposite coating.

4.4.2. Fourier-Transform Infrared Spectroscopy (FTIR)

The epoxy matrix, ZnO/epoxy, and GO/ZnO/epoxy nanocomposite samples were further inspected by FT-IR spectral analysis as shown in Figure 4.17 [a, b, and c], respectively. The epoxy matrix spectrum Figure 4.17a describes the characteristic absorption bands of the epoxy matrix. The absorption frequencies bands at 556, and 828.2 cm^{-1} are credited to the stretching vibration of the C-H bond [76]. The polymer backbone's C–O–C stretching vibration appears at 1031.9, and 1096.6 cm^{-1} [77]. Typical bands of aromatic C=C are related to the styrene units at 1605, and 1492 cm^{-1} [78]. The board absorption vibration bands between 2967.2 and 2860 cm^{-1} are ascribed to the asymmetric and symmetric stretching frequencies of -CH_2 [77]. Moreover, the board absorption band at 3429 cm^{-1} relates to the O–H stretching vibration [79]. The FT-IR spectra of ZnO/epoxy, as shown in Figure 4.17b indicate the identical absorption bands observed for the epoxy matrix and beside the extra specific band that corresponds to Zn–O–Zn stretching frequencies at 449.9 cm^{-1} possesses evidence of the existence of the ZnO nanoparticles, which agrees with previous studies [41]. The FT-IR spectra of GO/ZnO/epoxy, as shown in Figure 4.17c, demonstrates the effective combination of GO nanosheets with ZnO nanoparticles. A significant increase in absorption peak intensities and the broadness of previously identified bands indicates the presence of GO nanosheets with ZnO nanoparticles, particularly the distinguished broadband at 3429 cm^{-1}, which reveals the presence of the hydroxyl group in GO [80]. These spectral variations indicate enhanced interactions between the nanofillers and the epoxy matrix, participating in effective structural modifications within the hybrid nanocomposite coating.

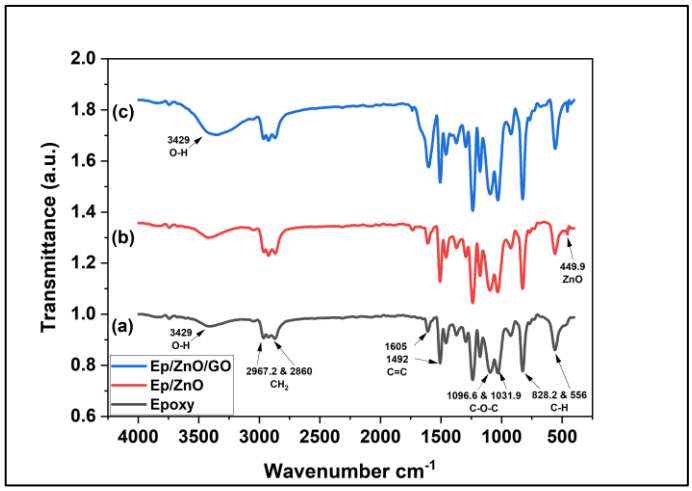

Figure 4.17. FTIR spectra of epoxy-coated substrate a), ep/ZnO coating b), and /ep/ZnO/GO coating c).

4.5. THERMAL CHARACTERIZATION

4.5.1. Thermogravimetric Analysis (TGA)

Thermogravimetric analysis (TGA) was examined for the Epoxy, ZnO/epoxy, and GO/ZnO/epoxy coatings under Nitrogen gas in a temperature range (25-800 ºC) and heating rate of 20 ºC/min, as shown in Figure 4.18. The thermal decomposition for each coating was observed over the broad temperature range. The thermal degradation process was followed for pure epoxy coating, which lost approximately 97% mass, and the remaining scrap mass was maintained at 3.3% by mass in the thermal degradation process up to 800 ºC. For ZnO/epoxy and GO/ZnO/epoxy coatings, revealing two major thermal decomposition steps, the first step is an optimised round at 290 ºC, matching the water molecules from the unhydrolyzed (Zn) network. The second step of decomposition of the sample was near the 345- 444 °C range, with a maximum at 380 ºC, appropriate to the consequent decomposition of the epoxy main chain. The remaining scrap mass maintained in the thermal degradation process at 800 ºC for ZnO/epoxy coating is 12.1%, corresponding with ZnO weighting. For GO/ZnO/epoxy coating, 15.1% by mass corresponds with ZnO and GO. This indication verifies the credibility of the preparation of the nanocomposite coating. The TGA test results in this study agree with previous literature studies [81].

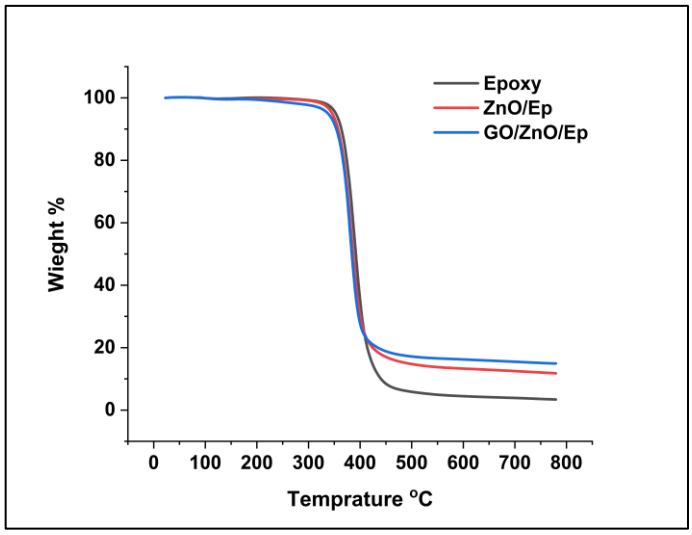

Figure 4.18. TGA curves of epoxy-coated substrate, ZnO/ep coating, and GO/ZnO/ep coating.

4.6. VICKERS MICROHARDNESS MEASUREMENTS

Vickers microhardness test results, as summarized in Table 4.11, provide essential insights into the mechanical performance of the fabricated composite coating systems. The GO/ZnO/epoxy sample exhibited the highest microhardness value of 29.3 HV/0.2/15, indicating superior surface resistance. In comparison, the ZnO/epoxy coatings demonstrated slightly lower values of 19.9 HV/0.2/15 and 20.1 HV/0.2/15. Both nanocomposite coatings showed significantly improved hardness over the pure epoxy coating, which recorded lower values of 11.6 HV/0.2/15 and 15.3 HV/0.2/15. The incorporation of ZnO nanoparticles and graphene oxide (GO) into the epoxy matrix significantly enhances mechanical properties, particularly hardness and resistance to deformation. The GO/ZnO/epoxy composite demonstrated superior performance due to GO's synergistic role in reinforcing structural rigidity and load-bearing capacity. These improvements align with previous studies on the beneficial effects of nanofillers in epoxy-based systems [82],[83].

Table 4.10. Vickers microhardness test results of epoxy-coated substrate, ZnO/epoxy coating, and GO/ZnO/epoxy coating

600	HBW	1/	30/	20	
					Duration Time of Test Force (s)
					Approximate Kgf Equivalent of Applied Test Force
					Ball Diameter in mm
					Hardness Symbol
					Brinell Hardness Value

Order	**Coating Sample**	**Results of Measurement**
		Microhardness tests
1	GO/ZnO/epoxy	29.3 HV/0.2/15, 29.3 HV/0.2/15
2	ZnO/epoxy	19.9 HV/0.2/15, 20.1 HV/0.2/15
3	epoxy	11.6 HV/0.2/15, 15.3 HV/0.2/15

4.7. SURFACE PROPERTY CHARACTERIZATION

4.7.1. Contact Angle Measurement (Wettability).

Contact angle tests were conducted to determine the hydrophobic or hydrophilic nature of the coating surfaces. These tests were used to evaluate the water resistance of the coating by analyzing the spreading behavior of water on the coating surface.
GO/ZnO/epoxy coatings exhibited higher contact angles than pure epoxy coatings, indicating that the coatings were more hydrophobic. Hydrophobic properties make it difficult for water to penetrate the coating surface, thus improving corrosion resistance. Contact angle tests confirmed that GO additive improved the water-repellence properties of the coatings.

These techniques used to characterise the coatings provided comprehensive information about the coatings' physical, chemical and thermal properties. SEM and FTIR analyses evaluated the coatings' surface structure and chemical bonding, while

TGA and microhardness tests revealed the thermal and mechanical strength of the coatings. Wettability tests evaluated the water resistance of the coatings. These results showed that GO/ZnO/epoxy nanocomposite coatings exhibit superior performance and offer significant advantages in corrosion protection and mechanical strength.

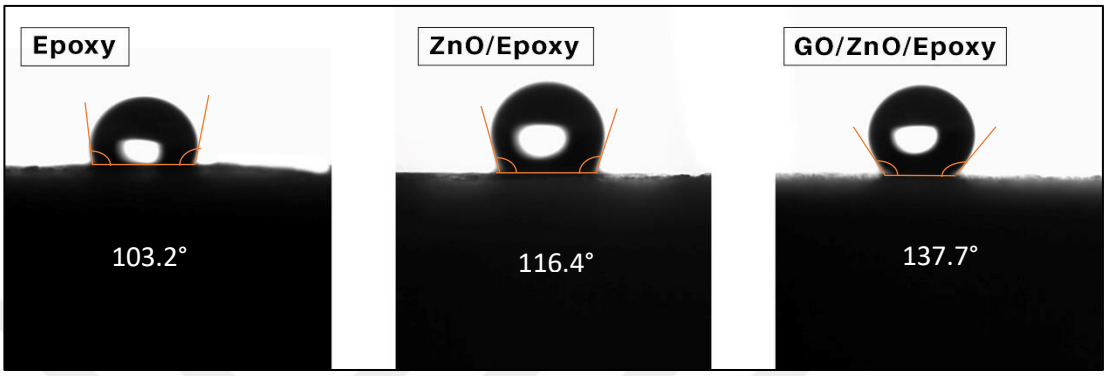

Figure 4.19. Contact angle of Epoxy coated substrate, ZnO/Epoxy coating and GO/ZnO/Epoxy coating.

CHAPTER 5

CONCLUSION AND FUTURE WORKS

The thesis has studied the boosting of epoxy coatings with zinc oxide (ZnO) nanoparticles and graphene oxide (GO) nanosheets for mechanical strength and corrosion resistance on magnesium substrate. The experimental results exhibited that the existence of such nanomaterials in epoxy coatings has significantly boosted performance, making them more sustainable for industrial activities involving corrosion environments.

The fruitfully applied ZnO nanoparticles, combined with the epoxy matrix in variable weight percentages, were made to improve the corrosion barrier by decreasing porosity and creating a hindrance path by which corrosive ions, such as chloride ions, are blocked. Among the sample tested, $ZnO_{4.1}$/ep showed the optimal corrosion barrier with the smaller corrosion rate 43.540 mmpy, thus demonstrating that an optimal filler loading could cause significant improvements in coating properties.

The optimized ZnO/epoxy matrix, after being formed, further promoted the superior properties of the coating system with the GO nanosheets. The electrochemical evaluation of Tafel and EIS plots revealed that coatings with GO nanosheets and ZnO nanoparticles exhibit much lower corrosion rates compared to the unmodified epoxy coating. Among the samples tested, $GO_{0.05}$/$ZnO_{4.1}$/ep showed the optimal corrosion barrier with the smallest corrosion rate 4.170 mmpy. The GO enhanced the electrochemical stability of the coating by decreasing the rate of charge transfer occurring along with the corrosion impacts. The Nyquist and Bode plot analyses essentially confirmed the superior performance of GO-modified nanocomposite coatings after extended exposure in a saline environment.

The SEM and EDX confirmed the observations by revealing a homogeneous distribution of ZnO and GO in the epoxy matrix, without evidence of micro-voids and large agglomerates. Also, EDX analysis proved the elemental composition of the nanocomposite coating. Furthermore, TGA and FTIR further testified to the thermal and structural stabilities of the coatings. The TGA revealed an increase in thermal degradation temperature in the nanocomposite sample, an indicator of enhanced thermal stability due to nanofillers. FTIR gave insights regarding strong chemical interactions existing between the epoxy matrix and the nanofillers, and especially functional groups within GO, which chemically bonded with the epoxy resin, thus further enhancing the coating's structural integrity and barrier characteristics.

Likewise, GO nanosheet with its large surface area and many functional groups would support mechanical reinforcement and adhesion between the nanofiller and epoxy matrix. This was proven by the higher microhardness of the GO/ZnO/Epoxy nanocomposite (29.3 HV) compared to the pristine epoxy (approximately 15.3 HV), confirming that GO preserves and enhances load-bearing ability and resistance to vertical deformation and wear.

This research advances knowledge on nanocomposite coatings and offers a practical approach to the fabrication of next-generation corrosion-resistant materials focused on making coatings that reduce maintenance costs, extend service life, and improve the safety of metallic infrastructure, which is a sustainable solution to the widespread problem of corrosion in harsh environments.

However, this research has sufficient data with the major advantages of incorporating ZnO nanoparticles and GO in epoxy coatings. It will be interesting for future work to investigate the long-term environmental durability of such nanocomposite systems in real industrial environments applied as a sense of field performance. One such capable area involves evaluating behavior under diverse pH, temperatures, and UV exposure to simulate marine, as well as chemical, and desert environments. This would give much more knowledge on nanocomposite stability and degradation mechanisms in various environments.

REFERENCES

1. Galliano, F., and Landolt, D., "Evaluation of corrosion protection properties of Additives for waterborne epoxy coatings on steel," Prog Org Coat, vol. 44, no.3,pp. 217–225 (2002).

2. Mišković-Stanković, V. B., Stanić, M. R., and Dražić, D. M., "Corrosion protection of aluminium by a cataphoretic epoxy coating," ***Prog Org Coat***, vol. 36, no. 1–2, pp. 53–63 (1999).

3. Wetzel, B., Haupert, F., and Qiu Zhang, M., "Epoxy nanocomposites with high mechanical and tribological performance," ***Compos Sci Technol***, vol. 63, no. 14, pp. 2055–2067 (2003).

4. Rong, M. Z., Zhang, M. Q., and Ruan, W. H., "Surface modification of nanoscale fillers for improving properties of polymer nanocomposites: A review," ***Materials Science and Technology***, vol. 22, no. 7, pp. 787–796 (2006).

5. Yamini, S., and Young, R. J., "Stability of crack propagation in epoxy resins," ***Polymer (Guildf)*****,** vol. 18, no. 10, pp. 1075–1080 (1977).

6. Perreux, D., and Suri, C., "A study of the coupling between the phenomena of water absorption and damage in glass/epoxy composite pipes," ***Compos Sci Technol***, vol. 57, no. 9–10, pp. 1403–1413 (1997).

7. Flor, G., Campari-Vigano, G., and Feduzi, R., "A thermal study on moisture absorption by epoxy composites," ***Journal of Thermal Analysis***, vol. 35, no. 7, pp. 2255–2264 (1989).

8. Meng, Y., Gao, H., Hu, J., and Gao, L., "Effect of pH value on the corrosion and corrosion fatigue behavior of AM60 magnesium alloy," ***J Mater Res***, vol. 34, no. 6, pp. 1054–1063 (2019).

9. Song, G., and Atrens, A., "Understanding Magnesium Corrosion—A Framework for Improved Alloy Performance," ***Adv Eng Mater***, vol. 5, no. 12, pp. 837–858 (2003).

10. Guo, L. F., Yue, T. M., and H. C. Man, H. C., "Excimer laser surface treatment of magnesium alloy WE43 for corrosion resistance improvement," ***J Mater Sci***, vol. 40, no. 13, pp. 3531–3533 (2005).

11. Internet: Zeng, R., "Science Review of studies on corrosion of magnesium alloys," Available: www.sciencedirect.comwww.csu.edu.cn/ysxb/ (2006).
12. Makar, G. L. and Kruger, J., "Corrosion of magnesium," *International Materials Reviews*, vol. 38, no. 3, pp. 138–153 (1993).

13. Ghali, E., Dietzel, W., and Kainer, K. U., "Testing of General and Localized Corrosion of Magnesium Alloys: A Critical Review," ***J Mater Eng Perform***, vol. 13, no. 5, pp. 517–529 (2004).

14. Pardo, A., Merino, M. C., Coy, A. E., Arrabal, R., Viejo, F., and Matykina, E., "Corrosion behaviour of magnesium/aluminium alloys in 3.5wt.% NaCl," ***Corros Sci***, vol. 50, no. 3, pp. 823–834 (2008).

15. Baril, G. and Pébère, N., "The corrosion of pure magnesium in aerated and deaerated sodium sulphate solutions," ***Corros Sci***, vol. 43, no. 3, pp. 471–484 (2001).

16. Pardo, A., Merino, M. C., Coy, A. E., Viejo, F., Arrabal, R., and Feliú, S., "Influence of microstructure and composition on the corrosion behaviour of Mg/Al alloys in chloride media," ***Electrochim Acta***, vol. 53, no. 27, pp. 7890–7902 (2008).

17. Santamaria, M., Di Quarto, F., Zanna, S., and Marcus, P., "Initial surface film on magnesium metal: A characterization by X-ray photoelectron spectroscopy (XPS) and photocurrent spectroscopy (PCS)," ***Electrochim Acta***, vol. 53, no. 3, pp. 1314–1324 (2007).

18. Schmutz, P., Guillaumin, V., Lillard, R. S., Lillard, J. A., and Frankel, G. S., "Influence of Dichromate Ions on Corrosion Processes on Pure Magnesium," ***J Electrochem Soc***, vol. 150, no. 4, p. B99 (2003).

19. Taheri, M., Phillips, R. C., Kish, J. R., and G. A. Botton, G. A., "Analysis of the surface film formed on Mg by exposure to water using a FIB cross-section and STEM–EDS," ***Corros Sci***, vol. 59, pp. 222–228 (2012).

20. Baril, G., Galicia, G., Deslouis, C., Pébère, N., Tribollet, B., and Vivier, V., "An Impedance Investigation of the Mechanism of Pure Magnesium Corrosion in Sodium Sulfate Solutions," ***J Electrochem Soc***, vol. 154, no. 2, p. C108 (2007).

21. Feliu Jr, S., Merino, M. C., Arrabal, R., Coy, A. E., and Matykina, E., "XPS study of the effect of aluminium on the atmospheric corrosion of the AZ31 magnesium alloy," ***Surface and Interface Analysis***, vol. 41, no. 3, pp. 143–150 (2009).

22. Feliu, S., Pardo, A., Merino, M. C., Coy, A. E., Viejo, F., and Arrabal, R., "Correlation between the surface chemistry and the atmospheric corrosion of AZ31, AZ80 and AZ91D magnesium alloys," ***Appl Surf Sci***, vol. 255, no. 7, pp. 4102–4108 (2009).

23. Nordlien, J. H., Ono, S., Masuko, N., and Nisancioglu, K., "A TEM investigation of naturally formed oxide films on pure magnesium," ***Corros Sci***, vol. 39, no. 8, pp. 1397–1414 (1997).

24. Lindström, R., Johansson, L.G., Thompson, G. E., Skeldon, P., and Svensson, J.E., "Corrosion of magnesium in humid air," ***Corros Sci***, vol. 46, no. 5, pp. 1141–1158 (2004).

25. Feliu, S., Maffiotte, C., Samaniego, A., Galván, J. C., and Barranco, V., "Effect of naturally formed oxide films and other variables in the early stages of Mg-alloy corrosion in NaCl solution," ***Electrochim Acta***, vol. 56, no. 12, pp. 4554–4565 (2011).

26. Feliu, S., Maffiotte, C., Galván, J. C., and Barranco, V., "Atmospheric corrosion of magnesium alloys AZ31 and AZ61 under continuous condensation conditions," ***Corros Sci***, vol. 53, no. 5, pp. 1865–1872 (2011).

27. Wang, L., Shinohara, T., and Zhang, B.-P., "Influence of chloride, sulfate and bicarbonate anions on the corrosion behavior of AZ31 magnesium alloy," ***J Alloys Compd***, vol. 496, no. 1–2, pp. 500–507 (2010).

28. Skar, J. I., "Corrosion and corrosion prevention of magnesium alloys," ***Materials and Corrosion***, vol. 50, no. 1, pp. 2–6 (1999).

29. Ugiansky, G., and Payer, J., "Stress Corrosion Cracking—*The Slow Strain-Rate Technique*. ASTM International100 Barr Harbor Drive", PO Box C700, ***West Conshohocken***, pp 19428-2959 (1979).

30. ZENG, R., "Review of studies on corrosion of magnesium alloys," ***Transactions of Nonferrous Metals Society of China***, vol. 16, pp. s763–s771 (2006).

31. Valente, T., "Grain boundary effects on the behavior of WE43 magnesium castings in simulated marine environment," ***J Mater Sci Lett***, vol. 20, no. 1, pp. 67–69 (2001).

32. Ghali, E., Dietzel, W., and Kainer, K.-U., "General and Localized Corrosion of Magnesium Alloys: A Critical Review," ***J Mater Eng Perform***, vol. 13, no. 1, pp. 7–23 (2004).

33. Ghali, E., "Corrosion and Protection of Magnesium Alloys," ***Materials Science Forum***, vol. 350–351, pp. 261–272 (2000).

34. Nordlien, J. H., Nisancioglu, K., Ono, S., and Masuko, N., "Morphology and Structure of Water-Formed Oxides on Ternary MgAl Alloys," ***J Electrochem Soc***, vol. 144, no. 2, pp. 461–466 (1997).

35. Song, G. L., and Atrens, A., "Corrosion Mechanisms of Magnesium Alloys," ***Adv Eng Mater***, vol. 1, no. 1, pp. 11–33 (1999).

36. Winzer, N., "A Critical Review of the Stress Corrosion Cracking (SCC) of Magnesium Alloys," ***Adv Eng Mater***, vol. 7, no. 8, pp. 659–693 (2005).

37. Potzies, C., and Kainer, K. U., "Fatigue of Magnesium Alloys," ***Adv Eng Mater***, vol. 6, no. 5, pp. 281–289 (2004).

38. Yue, T. M., Ha, H. U., and Musson, N. J., "Grain size effects on the mechanical properties of some squeeze cast light alloys," ***J Mater Sci***, vol. 30, no. 9, pp. 2277–2283 (1995).

39. Stephens, R. I., Schrader, C. D., and Lease, K. B., "Corrosion Fatigue of AZ91E-T6 Cast Magnesium Alloy in a 3.5 Percent NaCl Aqueous Environment," ***J Eng Mater Technol***, vol. 117, no. 3, pp. 293–298 (1995).

40. Finšgar, M., and Jackson, J., "Application of corrosion inhibitors for steels in acidic media for the oil and gas industry: A review," ***Corros Sci***, vol. 86, pp. 17–41 (2014).

41. Lv, K., Pan, R., Zhang, L., Tian, Y., Sui, Y., and Wan, D., "Synergistically assembled graphene/ZnO composite to enhance anticorrosion performance of waterborne epoxy coatings," ***RSC Adv***, vol. 12, no. 15, pp. 9069–9076 (2022).

42. Cross, R. B. M., De Souza, M. M., and Narayanan, E. M. S., "A low temperature combination method for the production of ZnO nanowires," ***Nanotechnology***, vol. 16, no. 10, pp. 2188–2192 (2005).

43. Gorrasi, G., and Vertuccio, L., "Evaluation of zein/halloysite nano-containers as reservoirs of active molecules for packaging applications: Preparation and analysis of physical properties**,"** ***J Cereal Sci***, vol. 70, pp. 66–71 (2016).

44. Ramezanzadeh, B., Attar, M. M., and Farzam, M., "A study on the anticorrosion performance of the epoxy–polyamide nanocomposites containing ZnO nanoparticles," ***Prog Org Coat***, vol. 72, no. 3, pp. 410–422 (2011).
45. Moghimi, N., Rahsepar, F. R., and Leung, K. T., "Supported binary hybrid nanomaterials and their applications," ***Coord Chem Rev***, vol. 320–321, pp. 82–99 (2016).

46. Yeh, J.-M., Weng, C.-J., Liao, W.-J., and Mau, Y.-W., "Anticorrosively enhanced PMMA–SiO2 hybrid coatings prepared from the sol–gel approach with MSMA as the coupling agent," ***Surf Coat Technol*****,** vol. 201, no. 3–4, pp. 1788–1795 (2006).

47. Zheng, S., and Li, J., "Inorganic-organic sol gel hybrid coatings for corrosion protection of metals," ***J Solgel Sci Technol***, vol. 54, no. 2, pp. 174–187 (2010).

48. Padinchare Covilakath, R. V., Cassidy, J., Oubaha, M., McDonagh, C., Colreavy, J., and Duffy, B., "Corrosion Protection Properties of Various Ligand Modified Organic Inorganic Hybrid Coating on AA 2024-T3," ***ECS Trans***, vol. 24, no. 1, pp. 231–246 (2010).

49. Andronic, L., Perniu, D., and Duta, A., “Synergistic effect between TiO2 sol–gel and Degussa P25 in dye photodegradation,” ***J Solgel Sci Technol***, vol. 66, no. 3, pp. 472–480 (2013).

50. Michiels, Y., Puyvelde, P., and Sels, B., “Barriers and Chemistry in a Bottle: Mechanisms in Today’s Oxygen Barriers for Tomorrow’s Materials,” ***Applied Sciences***, vol. 7, no. 7, p. 665 (2017).

51. Farooq, S. A., Raina, A., Mohan, S., Arvind Singh, R., Jayalakshmi, S., and Irfan Ul Haq, M., “Nanostructured Coatings: Review on Processing Techniques, Corrosion Behaviour and Tribological Performance,” ***Nanomaterials***, vol. 12, no. 8, p. 1323 (2022).

52. Pourhashem, S., Vaezi, M. R., Rashidi, A., and Bagherzadeh, M. R., “Exploring corrosion protection properties of solvent-based epoxy-graphene oxide nanocomposite coatings on mild steel,” ***Corros Sci***, vol. 115, pp. 78–92 (2017).

53. Nguyen, T. A., Nguyen, T. H., Nguyen, T. V., Thai, H., and Shi, X., “Effect of Nanoparticles on the Thermal and Mechanical Properties of Epoxy Coatings,” ***J Nanosci Nanotechnol***, vol. 16, no. 9, pp. 9874–9881 (2016).

54. Davis, A., Yeong, Y. H., Steele, A., Bayer, I. S., and Loth, E., “Superhydrophobic Nanocomposite Surface Topography and Ice Adhesion,” ***ACS Appl Mater Interfaces***, vol. 6, no. 12, pp. 9272–9279 (2014).

55. Sung L.-P., “Scratch behavior of nano-alumina/polyurethane coatings,” ***J Coat Technol Res***, vol. 5, no. 4, pp. 419–430 (2008).

56. Li, C.-J., Yang, G.-J., Gao, P.-H., Ma, J., Wang, Y.-Y., and Li, C.-X., “Characterization of Nanostructured WC-Co Deposited by Cold Spraying,” ***Journal of Thermal Spray Technology***, vol. 16, no. 5–6, pp. 1011–1020 (2007).

57. Luo, X.-T., and Li, C.-J., “Thermal Stability of Microstructure and Hardness of Cold-Sprayed cBN/NiCrAl Nanocomposite Coating,” ***Journal of Thermal Spray Technology***, vol. 21, no. 3–4, pp. 578–585 (2012).

58. Kim, J. S., “Cold spraying of in situ produced TiB2–Cu nanocomposite powders,” ***Compos Sci Technol***, vol. 67, no. 11–12, pp. 2292–2296 (2007).

59. Cho, S., “Multi-walled carbon nanotube-reinforced copper nanocomposite coating fabricated by low-pressure cold spray process,” ***Surf Coat Technol***, vol. 206, no. 16, pp. 3488–3494 (2012).

60. Wang, F., Arai, S., and Endo, M., “Electrochemical Preparation and Characterization of Nickel/Ultra-Dispersed PTFE Composite Films from Aqueous Solution,” ***Mater Trans***, vol. 45, no. 4, pp. 1311–1316 (2004).

61. Yuan, R., “Superamphiphobic and Electroactive Nanocomposite toward Self-Cleaning, Antiwear, and Anticorrosion Coatings,” ***ACS Appl Mater Interfaces***, vol. 8, no. 19, pp. 12481–12493 (2016).

62. Zhang, S., Sun, G., He, Y., Fu, R., Gu, Y., and Chen, S., “Preparation, Characterization, and Electrochromic Properties of Nanocellulose-Based Polyaniline Nanocomposite Films,” ***ACS Appl Mater Interfaces***, vol. 9, no. 19, pp. 16426–16434 (2017).

63. Kaboorani, A., Auclair, N., Riedl, B., and Landry, V., “Mechanical properties of UV-cured cellulose nanocrystal (CNC) nanocomposite coating for wood furniture,” ***Prog Org Coat***, vol. 104, pp. 91–96 (2017).

64. Bu, A., “Corrosion behavior of ZrO2–TiO2 nanocomposite thin films coating on stainless steel through sol–gel method,” ***J Solgel Sci Technol***, vol. 81, no. 3, pp. 633–638 (2017).

65. Figueira, R., Fontinha, I., Silva, C., and Pereira, E., “Hybrid Sol-Gel Coatings: Smart and Green Materials for Corrosion Mitigation,” ***Coatings***, vol. 6, no. 1, p. 12 (2016).

66. “Practice for Calculation of Corrosion Rates and Related Information from Electrochemical Measurements,” ***ASTM International, West Conshohocken,*** *PA* (2023).

67. Jiang F., “Anti-corrosion behaviors of epoxy composite coatings enhanced via graphene oxide with different aspect ratios,” ***Prog Org Coat***, vol. 127, pp. 70–79 (2019).

68. Yao, Z., Jiang, Z., and Wang, F., “Study on corrosion resistance and roughness of micro-plasma oxidation ceramic coatings on Ti alloy by EIS technique,” ***Electrochim Acta***, vol. 52, no. 13, pp. 4539–4546 (2007).

69. Rammelt, U., and Reinhard, G., “On the applicability of a constant phase element (CPE) to the estimation of roughness of solid metal electrodes,” ***Electrochim Acta***, vol. 35, no. 6, pp. 1045–1049 (1990).

70. Al-Rashed, O., and Nazeer, A. A., “Ionic liquid-assisted production of hydrophobic nanocomposite coating for mild steel corrosion prevention in saline medium,” ***Journal of Materials Research and Technology***, vol. 18, pp. 5087–5102 (2022).

71. Chopra, I., Ola, S. K., Priyanka, Dhayal, V., and Shekhawat, D. S., “Recent advances in epoxy coatings for corrosion protection of steel: Experimental and modelling approach-A review,” ***Mater Today Proc***, vol. 62, pp. 1658–1663 (2022).

72. Ikeuba, A. I., “AFM and EIS investigation of the influence of pH on the corrosion film stability of Al4Cu2Mg8Si7 intermetallic particle in aqueous solutions,” ***Applied Surface Science Advances***, vol. 11, p. 100291 (2022).

73. Yasar, M., “A study of epoxy-based polymer composites: Tailoring mechanical and piezoelectric characteristics,” ***Polym Compos***, vol. 46, no. 6, pp. 5669–5684 (2025).

74. Mostovoy, A., “Investigating the Structure and Properties of Epoxy Nanocomposites Containing Nanodiamonds Modified with Aminoacetic Acid,” ***Polymers (Basel)***, vol. 16, no. 4, p. 449 (2024).

75. Alamdari, S., “RETRACTED: Preparation and characterization of GO-ZnO nanocomposite for UV detection application,” ***Opt Mater (Amst)***, vol. 92, pp. 243–250 (2019).

76. Maity, P., Kasisomayajula, S., Parameswaran, V., Basu, S., and Gupta, N., “Improvement in surface degradation properties of polymer composites due to pre-processed nanometric alumina fillers,” ***IEEE Transactions on Dielectrics and Electrical Insulation***, vol. 15, no. 1, pp. 63–72 (2008).

77. Ramírez-Herrera, C. A., Cruz-Cruz, I., Jiménez-Cedeño, I. H., Martínez-Romero, O., and Elías-Zúñiga, A., “Influence of the Epoxy Resin Process Parameters on the Mechanical Properties of Produced Bidirectional [±45°] Carbon/Epoxy Woven Composites,” ***Polymers (Basel)***, vol. 13, no. 8, p. 1273 (2021).

78. Singho, N. D., Lah, N. A. C., Johan, M. R., and Ahmad, R., “FTIR Studies on Silver-Poly (Methylmethacrylate) Nanocomposites via In-Situ Polymerization Technique,” ***Int J Electrochem Sci***, vol. 7, no. 6, pp. 5596–5603 (2012).

79. Doblies, A., Boll, B., and Fiedler, B., “Prediction of Thermal Exposure and Mechanical Behavior of Epoxy Resin Using Artificial Neural Networks and Fourier Transform Infrared Spectroscopy,” ***Polymers (Basel)*****,** vol. 11, no. 2, p. 363 (2019).

80. Sudesh, N., Kumar, S., Das, C., Bernhard, and Varma, G. D., “Effect of graphene oxide doping on superconducting properties of bulk MgB_2,” ***Supercond Sci Technol***, vol. 26, no. 9, p. 095008 (2013).

81. Nazeer, A. A., Al Sagheer, F., and Bumajdad, A., “Aramid-Zirconia Nanocomposite Coating With Excellent Corrosion Protection of Stainless Steel in Saline Media,” ***Front Chem***, vol. 8 (2020).

82. Dong, Y., Sun, W., Liu, X., Ma, M., Zhang, Y., and Liu, Y., “Electrophoretic-Deposition of Graphene and Microstructure and Friction Behavior of Ni–Graphene Composite Coatings,” ***Adv Eng Mater***, vol. 21, no. 8 (2019).

83. Yasin, G., “Synthesis of spheres-like Ni/graphene nanocomposite as an efficient anti-corrosive coating; effect of graphene content on its morphology and mechanical properties,” *J Alloys Compd*, vol. 755, pp. 79–88 (2018).

CURRICULUM VITAE

Khaled ALJILOU. He completed his primary and secondary education in Riyadh and graduated from AL-Yamamah High School. In 2017, he began his undergraduate studies in the Department of Mechanical Engineering at Karabük University, from which he graduated in 2022. He subsequently enrolled in a master's program at Karabük University in 2022, focusing on Nanotechnologies and Their Applications on Materials, where he continues his academic studies.